ARMY RESEARCH LABORATORY

Loading-Strain Equivalence Between Thermomechanical, Creep, and Tensile Tests: High Density Polyethylene

Albert A. Warnas

ARL-TR-456 July 1994

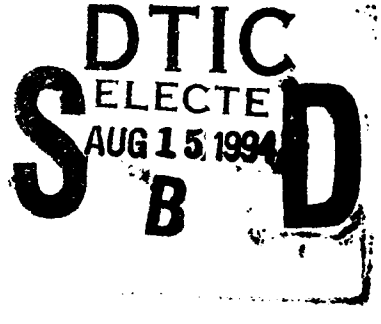

The findings in this report are not to be construed as an official Department of the Army position unless so designated by other authorized documents.

Citation of manufacturer's or trade names does not constitute an official endorsement or approval of the use thereof.

Destroy this report when it is no longer needed. Do not return it to the originator.

REPORT DOCUMENTATION PAGE

Form Approved
OMB No. 0704-0188

1. AGENCY USE ONLY *(Leave blank)*	2. REPORT DATE	3. REPORT TYPE AND DATES COVERED
	July 1994	Final Report

4. TITLE AND SUBTITLE
Loading-Strain Equivalence Between Thermomechanical, Creep, and Tensile Tests: High Density Polyethylene

5. FUNDING NUMBERS

6. AUTHOR(S)
Albert A. Warnas

7. PERFORMING ORGANIZATION NAME(S) AND ADDRESS(ES)
U.S. Army Research Laboratory
Watertown, MA 02172-0001
ATTN: AMSRL-MA-PA

8. PERFORMING ORGANIZATION REPORT NUMBER
ARL-TR-456

9. SPONSORING/MONITORING AGENCY NAME(S) AND ADDRESS(ES)
U.S. Army Research Laboratory
2800 Powder Mill Road
Adelphi, MD 20783-1197

10. SPONSORING/MONITORING AGENCY REPORT NUMBER

11. SUPPLEMENTARY NOTES

12a. DISTRIBUTION/AVAILABILITY STATEMENT
Approved for public release; distribution unlimited.

12b. DISTRIBUTION CODE

13. ABSTRACT *(Maximum 200 words)*

(See Abstract on Reverse - page ii.)

14. SUBJECT TERMS
Mechanical loading, Tensile test, Creep test, Thermomechanical test, HDPE

15. NUMBER OF PAGES
59

16. PRICE CODE

17. SECURITY CLASSIFICATION OF REPORT	18. SECURITY CLASSIFICATION OF THIS PAGE	19. SECURITY CLASSIFICATION OF ABSTRACT	20. LIMITATION OF ABSTRACT
Unclassified	Unclassified	Unclassified	UL

NSN 7540-01-280-5500

Standard Form 298 (Rev. 2-89)
Prescribed by ANSI Std. Z39-18
298-102

13. ABSTRACT

The initiation of any mechanical test, performed on a specimen of any material, requires first that the specimen be loaded. Any loading of a specimen causing it to deform may affect the test it initiates. The creep test (CT) is a dead-load test while the engineering tensile test (TT) is a pure loading test (load versus strain at constant crosshead-speed from its initiation to the yield point). In the CT, the specimen requires dead-load loading (DLL) at some DLL initial-crosshead-speed (HS) after which it creep-strains with time under a constant dead-load. In the literature, however, there is a neglect for loading (for example, neglecting to specify loading rates) in the CT. The assumption, in many cases, is that loading plays a minor role in creep-strain initiation so that loading effects can be precinded from regarding the remainder of the CT

This paper attempts to show that the loading parameters are very important for the initiation of the CT in plastics and that the loading mode has a bearing not only on the CT but also on the thermomechanical test (TMT).

Toward this end we performed three mechanical tests--on specimens of high density polyethylene (HDPE)--examining and comparing them regarding their loading dependence. The TT curves, in the e-t_L plane, had constant crosshead speed loading paths at constant temperature to point $R(L_o,T_o,e,t_L)$ where L_o is dead-load, T_o is test temperature, e is engineering strain, and t_L is the loading time. The DLL method initiated the CT and the TMT. The primary creep strain at the point $N = N(L_o,T_o,e,t_L)$ on the CT DLL strain path, in the e-t_L plane, was dependent on the DLL initial speed (HS). The CT DLL strain-path also initiates a TMT at N. We compared the data points from the two loading methods for loading strain equivalence. Equivalence occurs between the CT and the TMT at N on the CT strain path. This equivalence occurs when the TMT, heating-temperature rate ($\dot{T}$) at N properly matches the DLL HS. Proper HS-$\dot{T}$ matching is required to produce undistorted TMT curves. The comparison of N to R indicated an anomalous loading-strain equivalence between the CT (or the TMT) and the TT when N equals R.

We also extrapolated the experimental results through a loading model encompassing, theoretically, a wider testing range for possible future experimental direction.

CONTENTS

FIGURES.

INTRODUCTION

This paper deals with the loading of semicrystalline, high density polyethylene (HDPE) test specimens, in two loading modes for initiating three mechanical tests. It also examines the effects of these loadings on the initiated tests. The three tests are the creep test (CT), the thermomechanical test (TMT), and the engineering tensile test (TT). We made a comparison of the three tests with due regard to the loading deformation (strain).

The views in the literature vary considerably on what happens during the mechanical loading of a specimen for a mechanical test such as the CT.

The production of undistorted TMT curves requires an awareness of the necessity for proper HS-$\dot{T}$ matching for loading-strain (LS) equivalency between CT and TMT strain (and under certain conditions, between CT, TMT and TT strain). The production of variously distorted CT and TMT curves due to diverse loading methods--in which there is unawareness of the need for proper HS-$\dot{T}$ pairing--may be the rule rather than the exception in the general CT and TMT literature. Then, under such circumstances, the result is data, produced by diverse experimentalists with diverse apparatus at diverse facilities, often impossible to correlate for LS equivalency. Therefore, we suggest an approach somewhat as presented in this paper as a requirement for the attainment of undistorted databases on mechanical loading.

During a TT loading of a plastic, the strain at any point R below the yield point on the TT load-strain curve is the sum of the elastic and viscoelastic strain components (1-3). TT loadings are ramp loadings (4,5). However, loadings for other tests show wide interpretation. As examples: Bauwens-Crowett and Bauwens (6) state that "... creep loadings are a fast TT loading.". Ratner and Krasnova (7) state " ... there is no e_0-deformation 'at the instant of load application', as if creep set in after this instant; in reality there is a gradual transition from the initial increasing deformation to creep.".

In this paper, mechanical deformation experiments with HDPE specimens indicated that elastic strain and viscoelastic strain are separable in the deformation range considered.

To perform a CT or TMT the specimen must first be loaded. In this paper we used the dead-load loading (DLL) method for the CT and the TMT on plastic specimens. The specimen responds in time with the generation of a total CT/TMT loading strain e at N. This strain consists of a ramped, Hookean (elastic) strain, due to DLL to the full dead-load (L_O), followed by a transient, viscoelastic strain with the constant dead-load L_O. The elastic strain is zero at the start of the DLL strain-rate application; it is a maximum elastic strain $e_O(L_O)$ at the instant L_O is airborne--as it separates from the descending platform on which it rests. The transient, viscoelastic strain ensues in the specimen immediately--upon completion of the elastic response to L_O. This transient strain is the time response of the specimen to the full, constant dead-load. It is primary creep. At $e_O(L_O)$, the apparatus-driven strain-rate on the specimen becomes a decreasing transient-strain rate--driven by a constant dead-load. When the transient strain reaches N = $N(L_O,T_O,e)$ on the CT strain-path, a choice can be made as to the initiation of a TMT or the

continuation of the CT. If the initial loading temperature remains constant, the CT curve automatically continues. But if $\dot{T}$ is applied at N, the TMT ensues. $\dot{T}$ is applied on the CT DLL strain-path with T_0 and full dead-load L_0. At N there is an LS equivalence between the CT and the TMT. We show that the necessary condition for the initiation of a proper (undistorted) TMT at N occurs only when $\dot{T}$ matches the DLL initial speed of the CT loading-strain-path. The TMT strain at N consists of the CT DLL elastic and constant-L_0 transient strain. It constitutes the total uniform strain generated in response to the dead-load and temperature. The parameters involved in the TMT are monitored until the specimen exhibits failure (the end of uniform strain) signified by a somewhat sudden and severe strain increase (necking) or rupture in a narrow temperature interval.

Except for a few isolated cases; for example References (8-10), the TMT is virtually unexplored in the United States. The TMT has been primarily the domain of Soviet research (8).

The experimental apparatus used in Reference (9) crudely resembles the apparatus used in the experimentation for the CT and TMT of the present paper.

Bossu, et al. (11) obtained TMT curves for several plastics with a rheograph. Nielsen (8) also generated TMT curves; he favored and suggested generation of complete TMT curves because of the useful information they entailed.

The TT is ubiquitous in the field of mechanical testing of materials. Well-known and much used. It consists of the continuous loading of a tensile specimen, at constant crosshead speed and constant temperature, from zero strain to the yield point or the breaking point. The load (stress) versus strain and the load (stress) versus loading time can be monitored simultaneously.

The TT strain, which occurs in phase with the load, consists of initial elastic strain joined, in the R-point region of the TT curve, by elastic-viscoelastic strain. The TT load-strain phase differs from the CT or TMT load-strain phase; that is, the elastic strain is in phase with the load in a DLL, but the CT or TMT viscoelastic strain is a transient after application of the full dead-load to the specimen. This and other difference will be examined throughout the paper.

The comparisons of the TMT to the TT and the CT as presented in this paper are novel. The Soviet literature abounds with TMT's (12-16). Yet, as far as could be found in a cursory search, the present perspective (demonstrating the TMT-CT LS equivalence or the TMT-CT-TT LS equivalence anomaly) did not exist elsewhere. However a paper relating polymer creep curves and stress-strain curves in compression (17) and another on the comparison of PMMA data from a creep test, a tensile test and a thermomechanical test (18) is pertinent. Brüller and Schmidt (19) discuss several mechanical modes of loading PMMA. They do this in conjunction with the setting of linear viscoelastic limits for PMMA.

Closely related to the TMT is the heat distortion test (8) to obtain the heat distortion of sheet and film under constant load or the deflection temperature of a prism under flexural load. However, these tests usually obtain data at a point (8). Shapery and Lou (20) used the TMT

cursorily as a "creep test" at constant $\dot{T}$ to determine the softening temperature of a composite specimen with a specific load. Riga (21) used several of these techniques, along with Vicat softening temperature and thermomechanical analysis (TMA), to determine the creep properties of a group of plastics that he related to ASTM values.

The TMT and the TMA have a number of features in common.

The ideal lower limit of a TMT or TMA is a curve with strain due to thermal effects alone. Thermodilatometry (TDA) is close to such an ideal curve (that is, one with zero load on the specimen). Like the TMT, the TMA requires a load. The TMA load is very small. It is smaller than the smallest load allowed by the present TMT apparatus. Thus, the TMA extension test is the practical limit of the low-load end of a set of TMT curves.

The TMA test can measure the extension or penitration of a specimen versus temperature due to a minute load. The penetration mode of the TMA places a small, concentrated load, of the order of several grams, on a small piece of the material cooled to some initial test temperature. From this initial temperature, we heat the specimen at a constant $\dot{T}$ over a suitable temperature range. We record the localized surface penetration as the displacement of the concentrated load over an interval of temperature. The indentation becomes severe at some high temperature noted by a sharp displacement increase in a narrow temperature range. The temperature at the sharp displacement in a TMA, in both the penetration and extension modes, recalls the softening point temperature of the material.

The TMT parallels this procedure. However, it requires a different specimen geometry and different means of deformation measurement. We can generate a family of TMT curves starting with the smallest experimentally practical dead-load. We generate each curve of the family with an incremental increase in dead-load. We use a fresh specimen for each curve. The set of curves has a constant $\dot{T}$. The softening point temperature at the "knee" of a TMT curve decreases with the increasing dead-load. This is an effect similar to the reduced glass transition temperature as expressed by Robertson (22), Bryant (23), and Andrews and Kazima (24) for amorphous plastics. In the present case, for HDPE, we call it a reduced softening temperature.

PURPOSE

There are several purposes to this paper:

- To introduce the "loading problem" mentioned cursorily in Reference 25. Loading problem recognition resulted from the occurrence of distinct effects in a plastic specimen test due to mechanical DLL. The loading problem involves the examination of and the attempt to quantify the effects produced on a plastic specimen by the ensuing mechanical test after the initial loading conditions. The loading problem addresses the questions: When and where does loading-strain effects cease, and, where does the strain in a specimen due to a particular mechanical test begin and how does loading affect this strain? The tests of concern are the CT and the TMT. We also examine the TT, solely a loading test by nature, in the role of a loading mode for a CT or TMT.

- To introduce the TMT in three-dimensional (3-D) space with coordinates of strain, temperature, and time and, to introduce the CT into this 3-D space.

- To examine the conditions for the TMT-CT-TT LS equivalence at Q (where N = R) and the general TMT-CT LS equivalence at N that involves the requirement of matching the TMT $\dot{T}$ to the DLL HS (the initial speed). For comparison with DLL, We examine the TT (engineering load versus engineering strain) curve as a TMT or a CT loading path for HDPE.

- To present an extended (theoretical) model for CT-TMT LS equivalence in HDPE specimens using DLL in the uniform strain range.

- To present an example of the use of the TMT by obtaining the Troutonian viscosity of HDPE from TT-TMT LS equivalent data.

- To review results on the compensation time (t_c) for HDPE. These results for HDPE tend to point to a unity of certain aspects of the present experimental (macroscopic and continuum) approach to the more fundamental aspects as presented by McCrum (26) and others.

- To introduce the TMA as the lower limit to the TMT: to indicate the importance that thermal strain as produced by a TDA with "zero" load would have in establishing the ideal TMT lower limit. This ideal lower limit for the TMT (and TMA) would be a TDA with loadless thermal strain due solely to the linear coefficient of thermal expansion and temperature.

As we used some unfamiliar experimental approaches and techniques with the two loading modes and the three tests to obtain novel results, we deemed it worthwhile and appropriate to take the space in this paper to disclose more fully the test equipment, specimens, and experimental procedures. These disclosures, along with the exposition of inherent limitations of our experimental system and the experimental difficulties met with it, should make for better understanding of the paper and easier reproduction of the results.

TEST EQUIPMENT, MATERIAL, AND SPECIMENS

THERMOMECHANICAL AND CREEP TEST EQUIPMENT

The equipment for creep and thermomechanical testing is a creep unit with an environmental chamber (EC) as an integral part. The location of the upper part of the stainless steel extensometer, with sample, is in the EC. The lower part, with a linear variable differential transformer (LVDT) for precision strain measurement, and adjusting micrometer, is outside and below the EC and just above the dead-load. A microcomputer hard wired to the liquid nitrogen EC cooler controls and to the EC heater controls manages the cooling and heating temperature rates. Reference 25 presents further details on the CT and TMT equipment.

ENGINEERING TENSILE TEST EQUIPMENT

The equipment used for producing TT curves is a 20,000 psi Instron electromechanical, universal tester with a range of constant crosshead speeds, an Instron clip-on extensometer, and an environmental chamber. The Instron tester had 20,000 psi grips manually operated to secure a specimen in the load train.

MATERIAL

The material is semicrystalline HDPE produced in granular form and designated as EHM-6001 by Phillips 66 Company. Its number average molecular weight is 19,100 with a melt flow index of 0.15 g/sec and a density of 0.960 g/cc.

SPECIMEN PRODUCTION AND HISTORY

An injection moulding machine (25) made bar specimens of HDPE. The bars were 12.7 x 1.27 x 0.01375 cm^3 (5 x 1/2 x 1/8 in^2). The bars had a slight end-to-end taper in thickness. Also, there was material shrinkage and uneven cooling causing the bar specimens to have a slight curvature in their faces and along their edges. The bars probably had some material orientation of unknown detail and amount. X-ray diffraction analysis in transmission through the center of the gage length in untested specimens indicated 54.6% crystallinity with no orientation or residual stress in the crystalline phase. Therefore, we expect material orientation and residual stress to reside in the amorphous phase. We used the U.S. Army Materials and Mechanics Research Center (AMMC) streamline tensile specimen (SL) (25,27) almost exclusively for all the testing in this paper. We made the specimens by routing--from the bars described above--to a width of 0.635 cm in the 1.27 cm straight sided portion of the 2.54 cm gage length. From the ends of the straight portion of the gage length, the specimen gradually widens in curves toward the grip ends. We show the contour superimposed on Fig. 2. We found the SL shape to be useful for soft plastics, like HDPE, softened by sufficiently high test temperature--where the extensometer knife-edge pressure, as well as variations in specimen cross section, causes stress concentrations in the cross section. The streamline taper tends to minimize these effects except near melting in HDPE. That is, for temperatures between 120°C and 140°C where the specimen is very soft. Here along with other shapes, the SL shape becomes ineffective in the extensometer.

ASTM Standard 801, Test Methods D 638-86, and ASTM E-8 were used as a guide in all the tests.

We used the ASTM Type IV specimen only in the one hour creep-loading and creep-path experiments. They produced insignificant differences when compared to the results with SL specimens for the temperatures and stress involved: 9.19 MPa (1333 psi).

Experience showed that small, superficial nicks and/or scratches on the specimen edges and faces did not affect the test results. Likewise, sanding some of the edges of the routed SL

and ASTM Type IV specimen contours did not affect the test results. Large notches, however, deliberately inflicted, as with a file, tended to shorten the yield point strain.

PROCEDURE

We used a strip-chart recorder with chart speeds of 1 in/min to 20 in/min and 1 in/hour to 20 in/hour to record the strain output of the test versus real time. For the performance of the TMT's and CT's, the specimen, extensometer, dead-load (iron weights), and all rods and couplings of the load train were in line and suspended from a U-beam welded at its ends to the steel frame of the creep apparatus. The dead-load was applied through an electric motor coupled to a worm gear moving up or down a cantilevered elevator platform on which the dead-load rests. The downward motion of the elevator initiated the loading of a specimen. During loading, the slack disappeared in all couplings--such as those between the lower end of the specimen and the dead-load. The dead-load was subsequently air borne (separate from the elevator platform and hanging from the end of the extending specimen). The elevator stopped automatically after a noncritical space was achieved between the dead-load and the elevator platform. This arbitrary spacing was preset. There was only one constant DLL speed of 0.127 m/min (5in/min) available. Only part of this DLL speed was imparted to the specimen; the other part was absorbed by the load-train coupling. Then, the load-train coupling and the 7.62 cm, initial specimen length between testing machine grips affected the resulting DLL strain rate in the 2.54 cm gage length. This resulting initial strain rate was 0.0127 m/min per 6.35 cm initial, specimen effective-length (0.5 in/min per 2.5 inch initial, specimen effective-length). The effective length changed with temperature so that the imparted loading rate tended to change noticeably with the test temperature of the specimen, increasing as the temperature increased above 20°C and decreasing as the test temperature decreased below 20°C. We see this phenomenon as a skewing with temperature of the DLL portion of the CT or TMT curves.

We performed the TMT with microprocessor-controlled constant heating temperature rates of 1K/min and 4K/min. These rates were linear while those greater than 4K/min were nonlinear.

A source of strain error in the TMT was lack of initial synchronization between time and temperature when the TMT DLL was initiated at the desired TMT starting temperature: the heating temperature rate $\dot{T}$ was initially less than the prescribed 1K/min and there was a strain rate discontinuity due to loading. We minimized the synchronization error, largely, by producing a loadless $\dot{T}$ excursion about five minutes and 5°C below the desired TMT starting temperature to stabilize $\dot{T}$ in the specimen before loading for the TMT. In this paper, we refer to this procedure as the "synchronization maneuver" (SM). After the DLL, the TMT continues from N to completion.

The TT data from Reference 25 produced the R-path data for this paper. Before either type of mechanical test, we gripped both specimen types (the SL and the ASTM Type IV) such that at 20°C the initial specimen length between grips was consistently 7.64 cm with a 2.54 cm

gage length. This practice was important to reproduce the effective specimen gage length among machines and among tests (25).

We used engineering strain in all tests and calculated engineering stress with a constant cross-sectional area of 0.1935 cm^2 (0.03 in^2) in the ASTM specimens. In the SL specimens, we determined the cross-sections at the specimen middle. We did this for each specimen with the aid of a micrometer.

In performing a DLL for a CT or a TMT at a constant $\dot{T}$ with the described creep unit, it is important to recognize the source and role of w(i), with and without W(EX).

W(EX) is the external dead-load due to the iron weights applied to the load train of the specimen. W(EX) and w(i)--in sum or individually--represent the experimental dead-load L_o used in the DLL's to make a set of TMT or CT curves.

w(i) represents the smallest load for a CT or TMT that the creep unit can apply. w(i) is the 13.2 Newton (3lbf) "intrinsic" dead-load due to the weight of the lower part of the extensometer. Application of w(i) occurs to the mounted specimen upon vertical orientation of the extensometer in the load train. w(i) occurs spontaneously--with an unknown loading rate. Then, w(i) continuously acts on the mounted specimen as a tensile force, producing a small "implicit" strain at ambient temperature. We call this strain implicit because the extensometer does not record it. This implicit strain is of concern because it introduces strain errors into the TMT and CT if not isolated and accounted for. If the extensometer was of negligible weight, this implicit strain on the specimen would be zero before the setting of the extensometer strain to zero.

At 20°C, there is no measurable thermal strain in the gage length of the mounted specimen since it is in its normal ambient state; therefore, no thermal strain error occurs at 20°C upon setting the extensometer to zero strain. The implicit strain at 20°C--due to w(i)--consists of elastic plus negligible linear viscoelastic strain. This implicit elastic strain is lost at 20°C upon setting the extensometer zero. However, the position of the implicit strain on a strain-temperature plot is sensitive to temperature. Therefore, it can be exposed to measurement in the temperature intervals above and below 20°C relative to the zero strain set at 20°C. Above and below 20°C, the strains due to the simultaneous effects of w(i) and temperature and the thermal strain (sensitive only to temperature) occur together and are measured together. Together, they comprise the total strain Δ given by

$$\Delta = \alpha T_o + e[w(i),T_o] + e_o[w(i)]. \qquad \text{Equation 1}$$

The first term is thermal strain. It is the product of temperature and the linear coefficient of thermal expansion α. Here we assume α constant, independent of temperature. We present the second term qualitatively. It is the strain due to the simultaneous effects of w(i) and temperature. It is recoverable viscoelastic strain. The last term is the small elastic strain (zeroed-out at 20°C upon setting the extensometer zero) with postulated zero viscoelastic strain due to

w(i). Experimentally, it occurs before the second term. It is available for use in a strain correction if needed. Being elastic, it is obtainable by calculation from Young's modulus.

If w(i) was zero, Δ would be completely represented by the first term of Eq. 1. Δ would represent only thermal strain as though from a TDA with zero load. Then, a set of strain-temperature (e-T) TMT curves, which are TMA curves with finite loads, would progress from a TDA with zero load to TMT curves with incrementally increasing loads. As the dead-loads produce the TMT curves, then L_o = W(EX) would represents the dead-loads for a set of TMT curves, when W(EX) assumes weights from zero to any specified maximum for a limiting TMT curve.

The set of TMT curves of the present experimental setup, however, starts with a TMT curve with a Δ due to a nonzero w(i). The strain due to w(i), represented by the second (and last term) of Eq. 1, occurs simultaneously with the first term. This strain is not separable from the first term unless all component strains are known individually. The components, however, may be approximated as a function of T_o at constant w(i) and constant $\dot{T}$. Δ, as a function of T_o at constant w(i) and constant $\dot{T}$, is the lower-limit TMT curve of the present experimental setup.

The experimental procedure for obtaining the Δ (or any TMT) curve is to zero the extensometer at 20°C. Next the specimen is cooled to the designated starting TMT temperature at some constant, cooling-temperature rate. At the starting temperature, the extensometer is rezeroed. Then, the TMT is performed: the specimen, under load, is heated at a constant $\dot{T}$ to the designated final temperature.

To set all curves to the same zero-strain point at the start of each TMT, we reset the zero on the extensometer before heating. This experimental procedure with an additional step of loading the specimen with W(EX)--the magnitude of W(EX) with w(i), along with the given $\dot{T}$, determines the TMT curve--applies to the production of any TMT curve. Then, for any TMT curve, after resetting zero on the extensometer and after applying $\dot{T}$, we load the specimen with L_o = w(i) + W(EX) according to the synchronization maneuver (SM). Note that the loading of a specimen with only w(i) precludes the use of the SM. Also note that every TMT curve in this paper implicitly contains a Δ.

We will show (in the EXPERIMENTAL WORK (RESULTS) section) that the LS equivalence between a set of TT curves and a set of TMT or CT curves requires a thermal strain correction. The form of the correction is a subtraction of the first term of Eq. 1 from each experimental TMT curve,

Assuming a constant α over the specified temperature range, we obtained the first term of Eq. 1 separately. Then the strain in each corrected TMT curve is due to L_o = w(i) + W(EX)--with each succeeding TMT curve produced by an increment to W(EX). When the complete Δ represents the subtractive strain correction--used to adjust a set of TMT curves for LS equivalence with a set of TT curves--the result is a set of over-corrected TMT curves.

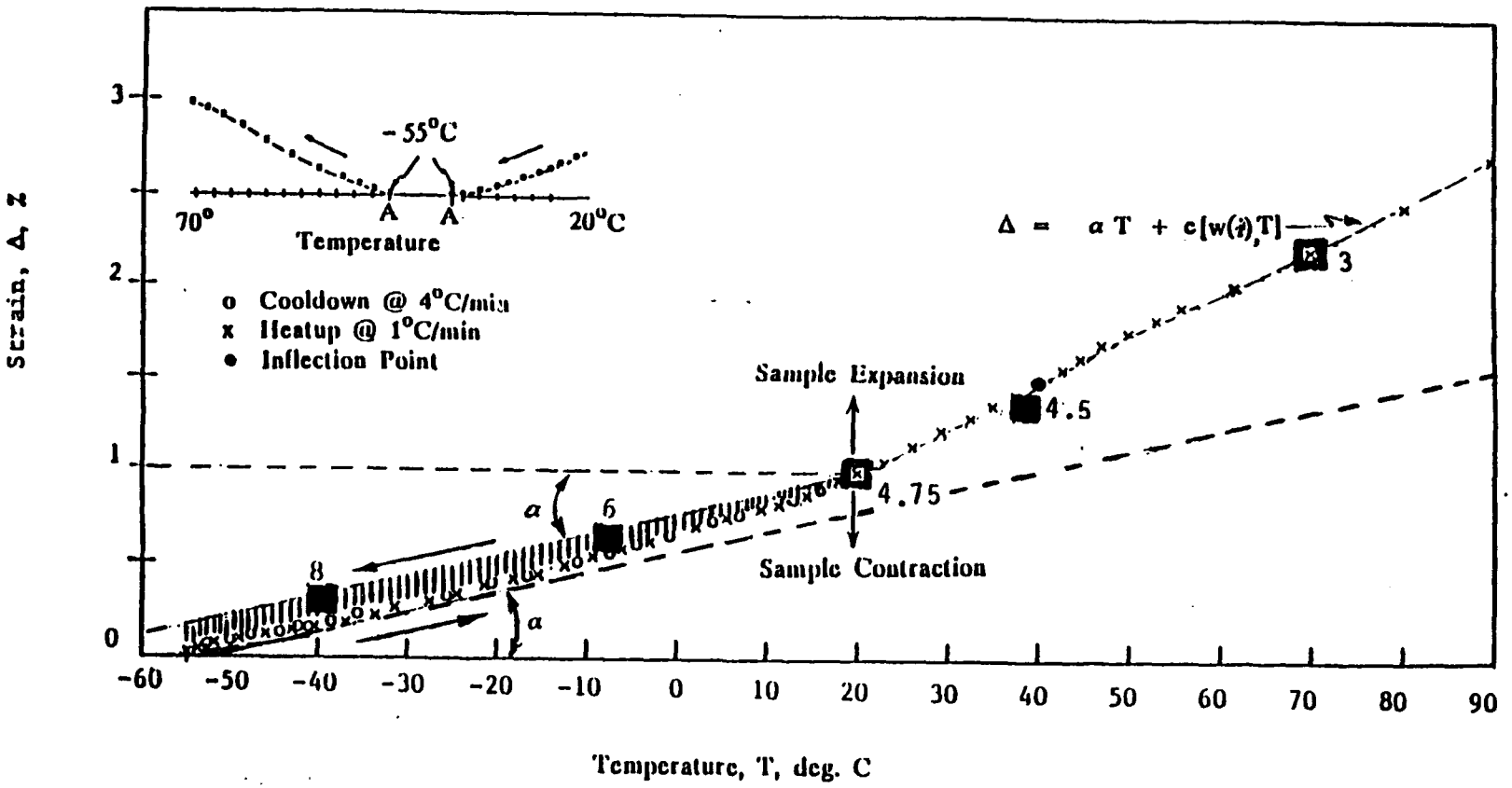

Fig. I. HDPE TMT curve (Eq. 1) under a dead-load w(i) = 13.2 Newton in the range -55°C < T_o < 70°C. $\dot{T}$ = 1 K/min.

EXPERIMENTAL WORK (RESULTS)

Fig. 1 is a plot of Δ versus T_o. Δ is given by Eq. 1. Fig. 1 represents a TMT curve, performed at a $\dot{T}$ of 1K/ min with a dead-load L_o of w(i). w(i) represents a stress of 0.69 MPa in the specimen cross section. The inset diagram shows the TMT curves for the cooling and heating temperature rates used to make this Δ versus T_o curve. Before cooling from 20°C, we set the experimental zero on the extensometer. The inset diagram shows the cooling path to -55°C at 4 K/min before heating at 1 K/min. The heating TMT curve (to the left of point A in the diagram) was replotted from point A to fold back onto the cooling TMT curve to Produce Fig. 1.

Upon cooling from 20°C to -55°C, contraction of the specimen occurred. Thermal strain, represented by the first term of Eq. 1, with a constant α, as seen in Fig. 1 (arrow left), causes part of the contraction. With the assumption of a constant α, the remainder of the contraction--the shaded part below 20°C--is the net viscoelastic strain represented by the second term of Eq. 1. This strain contraction is the difference between the extension due to w(i) and the contraction due to decreasing temperature. The circles in Fig. 1 represent the total contraction ($-\Delta$) upon cooling between 20°C and -55°C.

At -55°C, before the application of $\dot{T}$ = 1 K/min, we reset the experimental zero on the extensometer. By resetting zero at -55°C, we exposed Δ to measurement at temperatures above -55°C, relative to -55°C. Then the strains of the second term of Eq. 1, representing the implicit strain due to w(i), were found when a constant α was assumed in the first term; for example, by taking $\alpha = 110 \times 10^{-6}\ K^{-1}$ in the first term, the strains of the second term were known at all $T_o >$ -55°C relative to the zero strain set at -55°C.

Upon heating between -55°C and 20°C, the thermal strain responded with an expansion (lower dash-line and arrow right). The strain represented by the second term of Eq. 1 also responded by expanding. The combined strains comprised the expanding Δ-strain path (denoted by x's in Fig. 1) which followed the contraction path back to 20°C. At 20°C Δ was again in its original pretest state. Above 20°C both terms of Δ contributed to specimen expansion.

Although $e_o[w(i)]$ is zeroed-out and hence does not contribute to Δ (c.f. Fig. 1), it remains a constant strain throughout the cooling and heating cycle.

No significant difference in Δ was noted between the different heating and cooling $\dot{T}$'s.

Note the solid squares in Fig. 1 (we detail the source of these solid squares later in several places in this paper). These solid squares indicate Δ-strains produced by heating $\dot{T}$'s between 3 K/min and 8 K/min (indicated by the numbers next to the solid squares). Again, Δ was not significantly affected by any heating $\dot{T}$ applied between -55°C and 70°C.

The above experimental results indicate that the thermal strain is not affected by the $\dot{T}$. These indications agree with the results of Schartz (28), for polybutadiene, who showed with

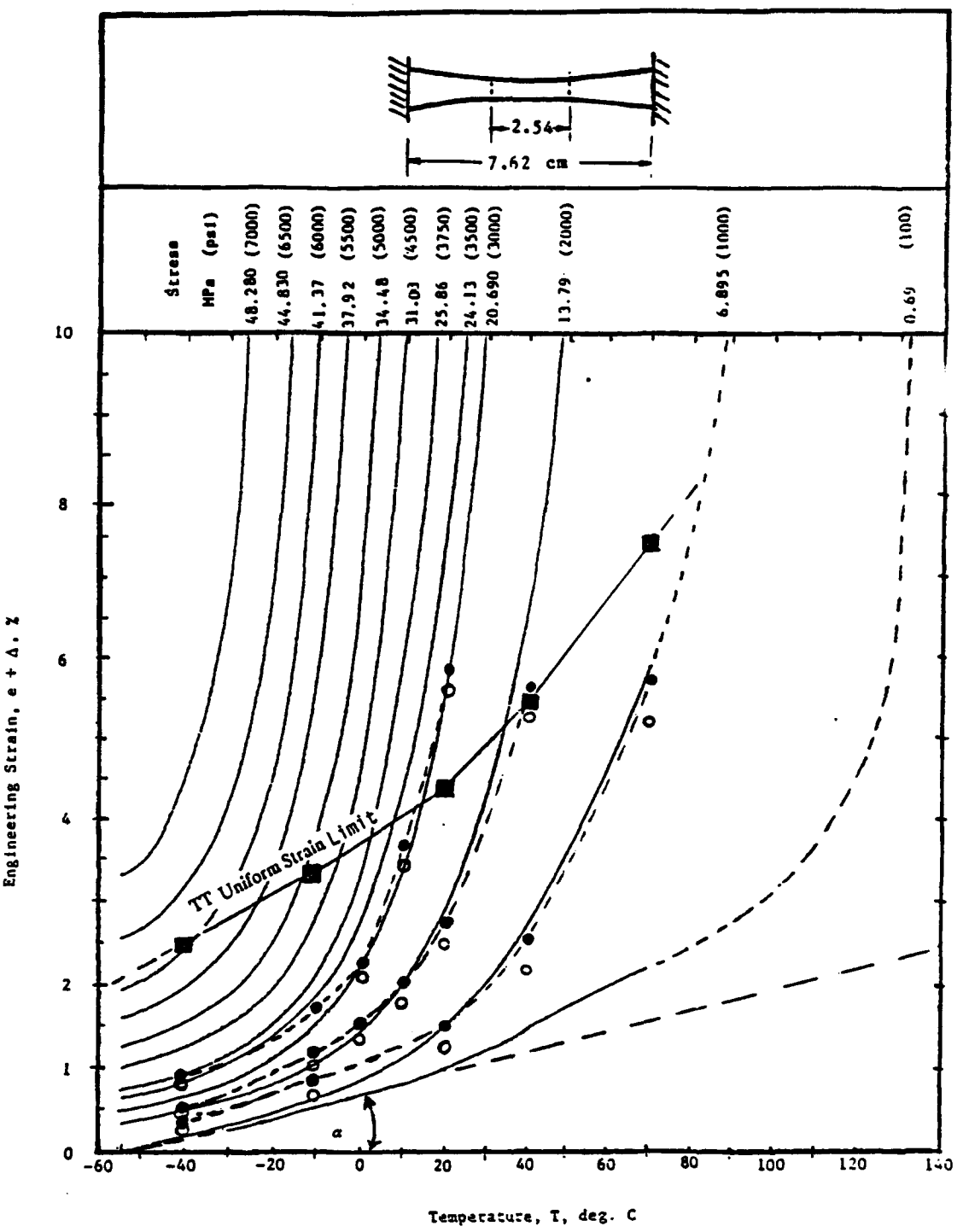

Fig. 2. HDPE TMT curves with indicated range of dead-loads and $\dot{T}$ = 1 K/min. Dead-load loading initial speed HS is 0.0127 m/min.

TMA that α was not affected by the heating and cooling rates (He also showed that specimen thickness did not affect α.).

As Fig. 1 is reminiscent of TMA, we consider some further thoughts about loading with TMA in the DISCUSSION section.

In this paper, the strain e in such expressions as $e\text{-}t_L$, $N(L_o,T_o,e)$, $de / d\tau$, etc., generically represents the total strain, comprised of all the mechanical and thermal components in a test curve.

Fig. 2 shows the TMT curves of engineering strain as a function of temperature for HDPE. We conducted the tests at a constant $\dot{T}$ of 1 K/min after loading each test with the SM at an effective initial speed of 0.0127 m/min (0.5 in/min) by the DLL method. We designate the initial speed, upon application of DLL, as HS throughout this paper. We reset the experimental zero on the extensometer before loading at -55°C, . The shift in speed, from 0.127 m/min to 0.0127 m/min, during loading was due to the combined effects of load-train softness, a specimen effective-length of 6.35 cm, and the skewing of HS with temperature. For each new curve we loaded a fresh specimen with a progressively increased constant dead-load. Each curve of Fig. 2 (in which we indicate the corresponding engineering stresses) contains the strains of Δ, given by Eq. 1. Δ versus T_o is the bottom TMT curve; it is detailed in Fig. 1.

The indicated stresses shown in Fig. 2 only hold to about the TT uniform-strain limit that we denote by connected solid squares (see the texts of Figs. 6 and 7). Uniform strain in the gage length of the specimen admits no localized (incipient necking) strains, and the specimen retains its shape below the uniform strain limit.

The TMT curves of Fig. 2 have the total strain, $e = e[L_o,T_o] + \alpha T_o$ due to temperature and to the load $L_o = w(i) + W(EX)$.

In Figs. 1 and 2, we used an α of 110×10^{-6} K^{-1}, an upper value for HDPE from the general literature, to isolate the thermal strain component of Δ by assuming α was a constant over the prescribed temperature range. In this form, we used the first term of Eq. 1 as the thermal strain correction on any family of TMT curves (provided a constant α over the prescribed temperature interval is acceptable).

Experiment showed that the thermomechanical strain at any point P on a TMT curve in Fig. 2, due to a dead-load $L_o = w(i) + W(EX)$, a test temperature T_o, and a $\dot{T}$ of 1 K/min, differed from the strain at T_o, for a specimen loaded to L_o in a TT with a crosshead speed of 1.27×10^{-3} m/min.

We will show in the text of Fig. 7 under what conditions a subtraction of thermal strain from the TMT curve made the TT-TMT strains equivalent. Actually, in Fig. 7, the reverse condition exists: since we constructed TMT curves from TT curves of Fig. 6 that are without thermal strain components, to make the constructed TMT curves comparable to those of Fig. 2

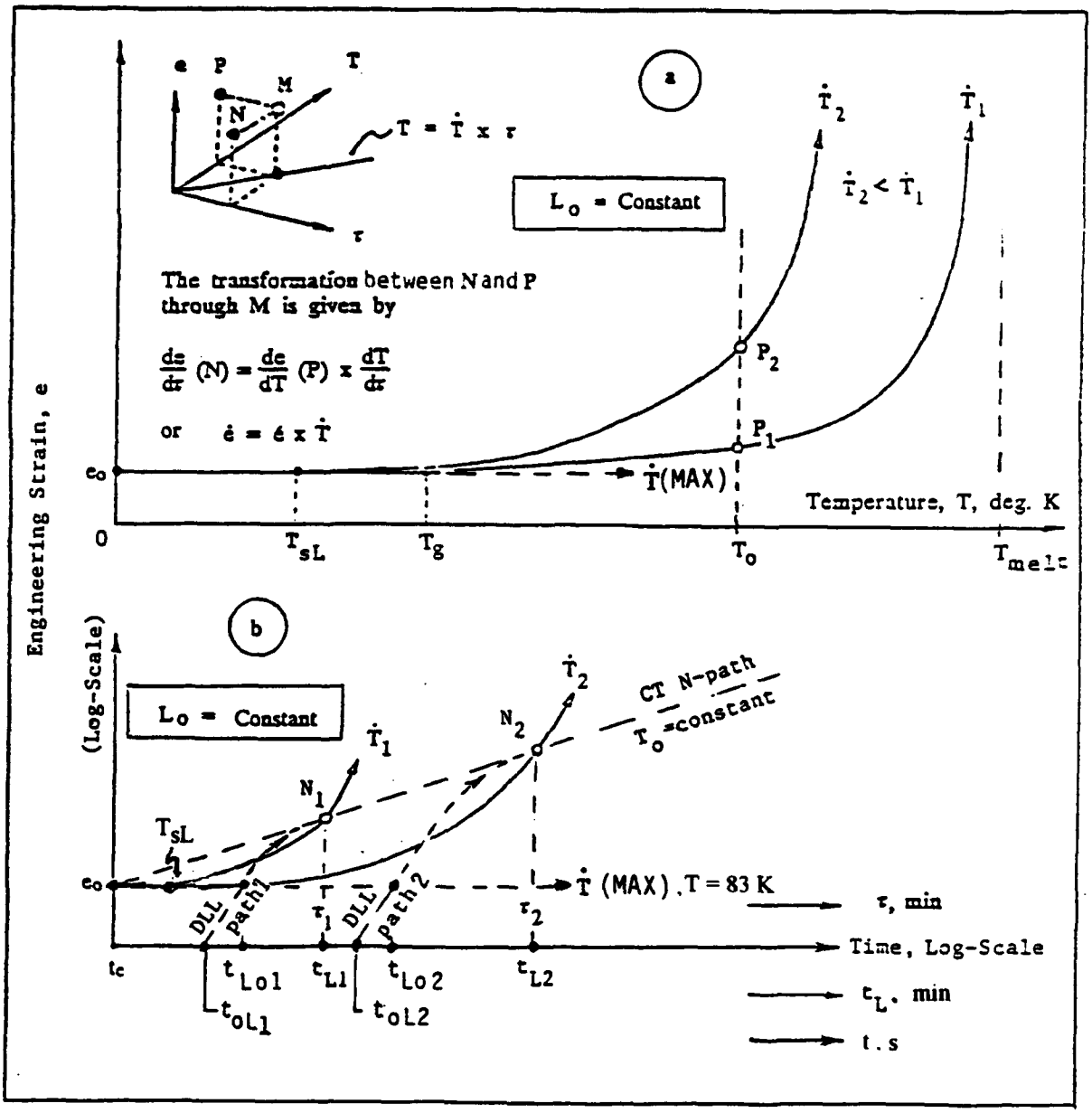

Fig. 3. Model for TMT-CT loading-strain equivalence in terms of TMT curve T-τ transformation. A typical CT N-path in the e-t_L plane is superimposed.

requires an addition of the thermal strain component with Eq. 1. Then, as in Fig. 2, the TMT curves of Fig. 7 have the strain $e = e[L_O,T_O] + \alpha T_O$, with the addition of the thermal strain. In Fig. 2, the solid circles indicate the constructed TMT curves fitted with an $\alpha = 110 \times 10^{-6}\ K^{-1}$ while the empty circles indicate the constructed TMT curves fitted with an $\alpha = 74 \times 10^{-6}\ K^{-1}$ Suffice it for now to point out that we found the congruence to be imperfect; we found congruence of the Fig. 2 TMT curves to the Fig. 7 TT(TMT) curves to exist only over the higher temperature ends of the TMT curves.

For direction to possible future experimentation, we present a model--represented by the combined Figs. 3, 4, and 5 and pertinent data from the references--that theoretically extends the experimental CT/TMT curves beyond the present limits of time and temperature. We also do this to show that the SM is still required when the TMT is loaded and initiated at $T_S \leq T_{SL}$. The advantage of being experimentally capable of loading in the T_S-τ_S region lies in the production of the "whole" TMT curve with a $\dot{T}$-HS match. A whole, or complete, TMT curve starts at $N_{SL} = N(L_O,T_{SL},e_O,\tau_{SL})$ and contains both the elastic and the viscoelastic strain. A TMT curve is completed when its strain reaches the TT uniform-strain limit at T(Neck) (where Neck stands for the end of the TT uniform strain limit). We treat the theoretical results obtained, due to the extension of the curves beyond experiment, in more detail in the DISCUSSION section.

We now consider Fig. 3. So far, we have described the TMT curve in the e-T plane that we show schematically in Fig. 3a --over an extended temperature range. We also show a schematic for the model--which describes the TMT N-path in the e-τ plane and the CT N-path in the e-t plane--in Fig. 3b. We represent the CT/TMT DLL curves tangent to the N path by a third set of time coordinates in the e-t_L plane. The CT and TMT N-path curves in Fig. 3 represent "whole", or complete, curves--initiated by DLL at appropriate extremes of high and low temperature and very short time that is not possible with the apparatus described in this paper. The model presents these N-path curves as sharing N-points common to the CT and TMT DLL curves. The TMT and the CT in Fig. 5 also share the M-point of any DLL path in an e-t_L plane that is perpendicular to the e-T plane for any given T.

We describe a point M (shown in the inset of Fig. 3a) on the TMT-CT surface, with prescribed constant dead-load L_O and constant heating temperature rate $\dot{T}$, by strain e, temperature T_O, and time ($t_L[\tau]$ for the TMT and $t_L[t]$ for the CT) coordinates. These orthogonal coordinates comprise a three-dimensional (3-D) space shown in Fig. 5.

We see that points on the TMT curves in Figs. 3a and 3b are orthogonal projections onto the e-T plane at P and the e-τ plane at N from the TMT/CT M-point surface in Fig. 5. Also, any CT curve is the orthogonal projection from the TMT/CT surface of Fig. 5 onto the e-t plane at N in Fig. 3b. Together, Figs. 3 and 5 comprise the model for the CT/TMT LS equivalence.

In 3-D space, CT curves occur in parallel e-t planes orthogonal to the e-T plane at their respective temperatures (see the text of Fig. 5). M is common to both the TMT and CT curves at their intersections in a 3-D milieu. Therefore, we consider the e-t and e-τ plane planar in Fig. 3b.

In Fig. 3b, the CT and TMT curves intersect at the common total-loading-strain e at the point N = $N(L_O,T_O,e,t) = N(L_O,e,\tau)$, when we project the DLL-plane (that is, the e-t_L plane) onto the planar e-t and e-τ planes.

The M-point orthogonal projection onto the T-τ plane is further described by the linear relation

$$T = \tau(dT / d\tau) = \tau\dot{T}, \qquad \text{Equation 2a.}$$

Where τ is the heating time.

Through any point $M = M(L_O,T,e,t_L[\tau])$, on a constant-load surface in the CT-TMT 3-D space, a point $P(L_O,T,e)$ in the e-T plane and a point $N(L_O,e,\tau)$ in the e-τ plane is found to be reversibly transformable (by an M to P or a P to M orthogonal transformation). These reversible, orthogonal-strain-projection transformations apply to the TMT curve and are dictated mathematically by the T-τ variable transformation

$$de / d\tau = (de / dT)(dT / d\tau) \text{ or, } \dot{e} = e'\dot{T}, \qquad \text{Equation 2b.}$$

The inset in Fig. 3a concerns Eqs. 2a and 2b and sketches how the TMT T-τ reversible transformation works for P and N through M in Figs. 3a and 3b.

We may orthogonally project strain in a TMT curve from the e-T plane to the e-τ plane by the transformation of T and τ through Eq. 2a. Eq. 2a implies that every constant $\dot{T}$ has its own family of TMT curves, like those in Figs. 2 and 3a (e versus T) or those in Fig. 3b (e versus τ) by a P to M to N reversible transformation.

We show the resulting TMT curves from such projections in Figs. 3a and 3b; that is, the strains at the P-points in Fig. 3a (for example, P_1 and P_2) are equivalent to the strains at the N-points (N_1 and N_2) of Fig. 3b.

In Figs. 3a and 3b, we are concerned with the reversible transformation of TMT strain from M to P or from M to N produced by the orthogonal projection of strain at M onto the e-T or e-τ plane, respectively. Also in Fig. 3b we are concerned with the orthogonal transformation of CT strain from M to N on the e-t plane.

In Figs. 3a and 3b, w(i) is zero. That is, we assume the extensometer weightless, and neglect the thermal strain αT_O for simplicity. Then, Δ is zero and the total strain e is $e(L_O,T_O)$ due to a total dead-load $L_O = W(EX)$, where W(EX) takes on all values from zero to a practical maximum W(MAX).

Tg in Fig 3a is the glass transition temperature.

We will summerize so far what we have said about Figs. 3 and 5. Fig. 3a represents the CT-TMT e-T curves, over the temperature interval 0 K < T < T(Neck), resulting from a DLL at T_S (called the TMT-curve "loading-source temperature" in this paper) in the interval 0 K < $T_S \leq T_{SL}$ = 83 K (see the DISCUSSION section for further details). Fig. 3b is the double-log plot of the TMT curves of Fig. 3a projected onto the e-τ plane (perpendicular to the T-axis at 0 K) in the time interval $t_c \leq \tau < \tau$(Neck) by a P to M to N transformation, as described in the inset of Fig. 3a. $t_c = 34 \times 10^{-6}$ s is the compensation time (its source is indicated in Fig. 4). Fig. 3b also shows the CT e-t_L plane superimposed on the TMT e-τ plane. Furthermore, Fig. 3b shows the CT N-path in the e-t plane. Therefore, for a DLL in an e-t_L plane to any M in the time interval $t_c \leq t_L < t_L$(Neck), N is the projection of M onto the CT e-t plane, or the TMT e-τ plane or the DLL e-t_L plane. For these three planar planes, the strain axes are identical while the time axes are not normalized (due to the choices we made in plotting the data particularly in Fig. 4), except at N_O where $t_c = t = \tau = t_L$ and where T = 0.002 K (similar to 0 K) with $\dot{T}$(MAX). It is seen that the shortest and quickest "instantaneous" DLL-path for a TMT (or a CT) is to $N_O = N(L_O,e_O,t_c)$. This DLL path is temperature independent as is the point N_O. From this DLL path or from any other DLL curve with HS_1 in the interval HS(MAX) > $HS_1 \geq$ HS(at Q) in the e-t_L plane to any $N(L_O,T_O,e,t_L)$, where N is in the interval $N_O < N < Q$ (the point Q is defined in the text of Fig. 4), theCT/TMT curves have a common N-point. Beyond N the TMT and CT curves have separate paths for the same temperature and load (stress level). Note, again, that the TMT and CT N-paths INTERSECT at $N = N(L_O,T_O,e,\tau[t_L]) = N(L_O,T_O,e,t[t_L])$ and that $t \neq \tau$ (when these paths are projected from M to N). Intersection at N between TMT and CT curves denotes loading-strain (LS) equivalency. The location of a typical CT N-path, shown in Fig. 3b, is also shown in Fig. 3a at To (in the TMT SM range) as the dash line, CT P-path isotherm, where both paths have the same dead-load. While the CT paths are isothermal, the TMT P and N paths are not.

The TMT curve passing through N is denoted by $\dot{N}(TMT \rightarrow \tau) = N(L_O,e,\tau) = P(L_O,T_O,e)$ and the CT curve passing through N is denoted by $N(CT \rightarrow t) = N(L_O,T_O,e,t)$. Now, from a DLL the N(TMT[with SM]) = N(CT) = $N(L_O,T_O,e,t_L)$ which is a point on the N-path (this is read: the N-point for a TMT is equivalent to that for a CT with the common parameters L_O,T_O,e and loading time). Therefore, the loading time t_L to any N along a common DLL path, is the same for the TMT as the CT curve. The DLL curve in the e-t_L plane and the CT N-path in the e-t plane are naturally connected, while the DLL curve is a separate phenomenon for the TMT curve.

The experimental TMT curves are shown in Figs. 1 and 2. They have the form depicted in Fig. 3a. They were loaded at $T_O = -55^oC >> T_{SL}$.

Fig. 3b shows DLL's to N_1 and N_2 along paths 1 and 2. In Fig. 3b, any τ-time, like τ_S or τ_O, for any $N(L_O,T_O,e)$ on the TMT path is reckoned from t_c and is defined by Eqs. 2a and 2b. In Fig. 3b, τ_O at N_1 and N_2 is denoted as τ_1 and τ_2.

Using Figs. 3a and 3b, we now introduce some further notation and definitions for the DLL of a specimen to N on the TMT curves, primarily in the SM temperature region To $\geq T_{SL}$ (and consequently for $\tau_O \geq \tau_{SL}$) where τ_O is associated with T_O through Eq. 2:

The temperature intervals 0 K < $T_S \le T_{SL}$ and $T_{SL} \le T_O$ < T(Neck) comprise the interval 0 K < T < T(Neck). The associated τ-time intervals are treated in the same way.

t_{oL1} is the starting time for the DLL along path 1 (see Fig. 3b) at which time the starting dead-load is zero (actually, the starting time is at t = 0, as shown in Fig. 10).

t_{Lo1} is the time along the DLL path 1 to the end of the DLL HS. It is the time for the development of the full load Lo which produces the elastic strain $e_o(L_o)$. At the end of t_{Lo1}, the transient, viscoelastic strain e_{VE} (primary creep) commences under L_o and proceeds along the transient viscoelastic (primary creep) part of the DLL path to N_1 in the time given by the difference between t_{L1} and t_{Lo1}.

t_{L1} is the DLL time t_L to $N_1(L_o,T_o,e_1)$ along path 1 from t_{oL1}.

The DLL path to any N on a CT/TMT curve has two components of strain: Hookean (elastic) strain and transient viscoelastic strain. The elastic strain is in phase with the dead-load. For the same L_o, the same elastic strain $e_o(L_o)$ is always obtained with a DLL from any HS. The transient viscoelastic strain occurs after the full dead-load is applied to the specimen. At t_{Lo} (see Fig. 3b), at the full dead-load L_o when the elastic strain is a maximum $e(L_o)$, HS on the elastic strain has become a minimum, associated with the strain rate $e_o(L_o)/t_{Lo}$. The transient viscoelastic strain starts immediately after $e_o(L_o)$ at t_{Lo} with the strain rate $e_o(L_o)/t_{Lo}$, proceeds to N --in the time t_L-- where it blends tangentially with the CT N-path. At N the transient strain rate has decreased monotonically to e/t_L. This also holds for DLL's in the SM temperature region To > T_{SL}.

The SM is necessary for the production of a segment of a whole TMT curve starting at T_o in the temperature range $T_{SL} < T_o <$ T(Neck) with the requirement that HS and $\dot{T}$ match at N, at the start of the segment. A DLL with HS ≤ HS(MAX) to any N along a TMT curve in this temperature range requires a correct $\dot{T}$ for a proper $\dot{T}$-HS match at N. An HS and $\dot{T}$ are properly matched at N if they follow the HS-$\dot{T}$ relation in Fig. 8. Therefore, a TMT or CT is considered undistorted if it is associated with a proper HS-$\dot{T}$ match. An HS-$\dot{T}$ match is also proper if the match produces CT-TMT LS equivalence at N.

The SM is required to start a TMT curve at any $P = P(L_o,T_o,e,\tau_o)$ in the e-T plane to match a whole TMT curve started at the LS TMT point $P_{SL} = P(L_o,T_{SL},e_o,\tau_{SL})$ with $\dot{T}$ chosen in the T_S-τ_S region; that is, the SM produces a segment of the whole TMT curve. The production of a segment of a whole TMT curve to commence at $T_o > T_{SL}$ requires a foreknowledge of the correct HS at T_o to match the $\dot{T}$ chosen in the T_S-τ_S region for the production of the whole TMT curve. Therefore, a database between HS and $\dot{T}$, like that established in Fig. 8, is required. This data can only be produced through careful experimentation using the model of Figs. 3 and 5 as a guide.

With care, the SM allows the high-temperature segment of a proper TMT curve to be produced. The TMT segment can be started with a DLL at the temperature To >> T_{sL} which is relatively easy to attain with modest experimental apparatus. We produced such segments for this paper.

At N, the TMT strain rate differs from the DLL transient-strain rate. Therefore, during the SM, upon changing from the DLL transient-strain rate to the TMT strain rate (or to the TMT $\dot{T}$) in Eq. 2b, a strain discontinuity occurs at N (and P).

A DLL ignoring the requirement that the DLL HS match a chosen $\dot{T}$ is an improper loading procedure. It will result in a distorted TMT curve when compared to a proper (undistorted) TMT curve started with the SM at N_S (or P_S); or, when compared to one started at N (or P) with the SM at To > T_{sL} with a proper HS-$\dot{T}$ match.

This is the case with the set of TMT curves of Fig. 2. .Each curve of Fig. 2 is a segment of a whole TMT curve. The Fig. 2 curves are produced with the existing HS of 0.0127 m/min which is mismatched (due to apparatus limitations) to the accompanying $\dot{T}$ of 1 K/min (see Fig. 8 text). This set of TMT curves, however, was found to be partially congruent to the TMT set in Fig. 7 constructed from the TT set of Fig. 6.

This partial congruence of the curves of Fig. 2 to those of Fig. 7 was found with αT_o (α = 110 x 10^{-6} K^{-1}) added to the strains of the curves in Fig. 7. These curves of Fig. 7, adjusted for thermal strain, are shown in Fig. 2 by the dash lines connecting the solid circles. This partial congruence, of the Fig. 2 to the Fig. 7 curves, excludes congruence in the initial, low temperature part of a TMT curve. For example, exclusion occurs from -55°C to about 20°C in the 6.9 MPa curve. These findings on partial congruence appear to indicate that an incorrect choice of DLL HS to match a chosen $\dot{T}$ results in a TMT curve initially distorted but which self-corrects over time with increasing temperature; that is, it becomes progressively a less distorted TMT curve as it tends to its high temperature end with $\dot{T}$, chosen at the start of any TMT, held constant throughout the TMT curve.

The requirement that HS properly match $\dot{T}$ (according to the prescription in Fig. 8) is a necessary one for producing undistorted TMT-CT LS equivalent curves that are reproducible . This condition and the requirement of uniform strain in the specimen are the necessary and sufficient conditions for TMT-TT LS equivalence. Note: Since uniform strain in the gage length of the specimen admits no localized (incipient necking) strains and the specimen retains its shape below the uniform strain limit, we expect that LS equivalence will occur only in the uniform strain range (see the text of Fig. 7).

We will address again the considerations in the last four paragraphs in the texts of Figs. 6 and 7.

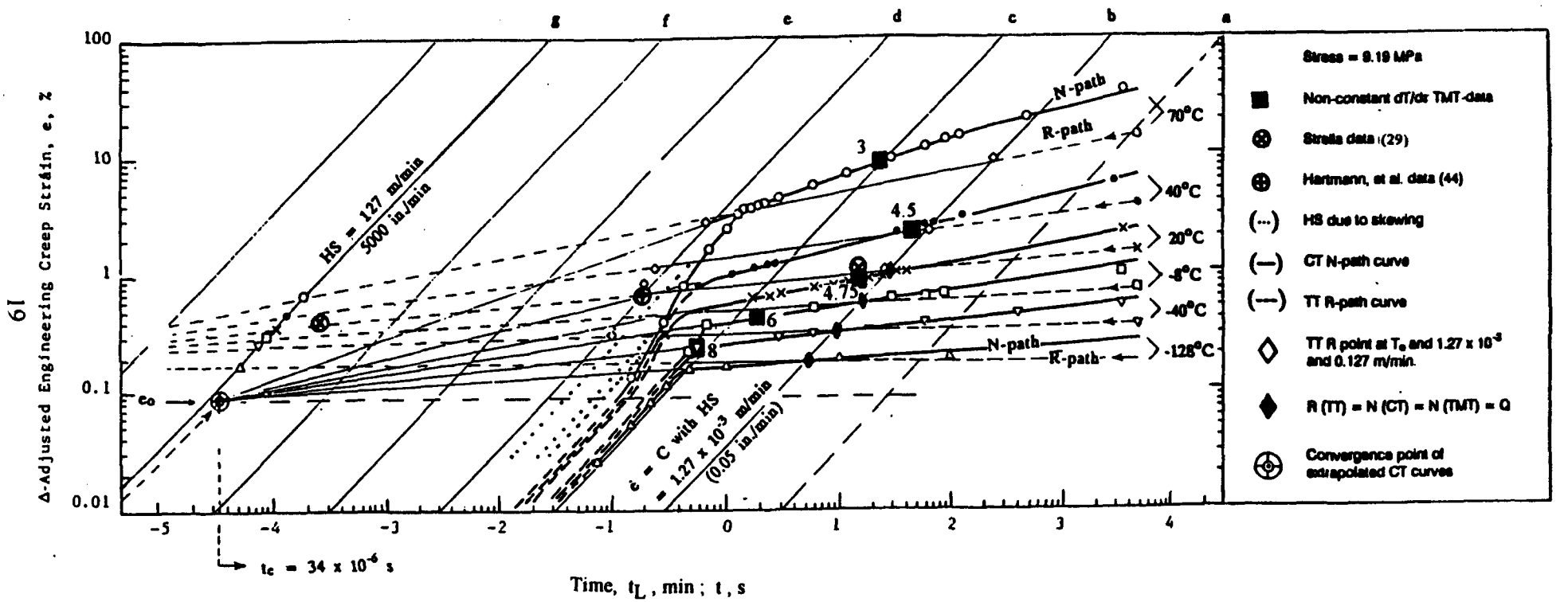

Fig. 4. CT N-path data, at the indicated temperatures and a stress of 9.19 MPa, extrapolated to N_O = N(9.19 MPa, T_O, e_O, t_C). TT data at the indicated loading speeds is superimposed.

Fig. 4 shows CT curves loaded for one hour at a stress level of 9.19 MPa (1333 psi) at several temperatures. These engineering-strain versus DLL time curves (e-t_L plane) and CT N-path curves (e-t plane) are on a double-log graph. Fig. 4 illustrates the DLL-mode results upon loading a specimen for a mechanical CT at $T_O > T_{sL}$.

Prior to each DLL at a specified T_O, Δ was automatically subtracted from the CT strain upon extensometer re-zeroing. Therefore, so there be CT-TT LS equivalence at the specific temperatures in Fig. 4, we added the strains of the second and third terms of Eq. 1 (from Fig. 1) to the CT strains.

At the stress level of 9.19 MPa, the strain of these CT curves was mostly in the uniform strain range. The elevator platform speed (HS) was 0.127 m/min (5 in/min). This is the only speed that the CT apparatus is equipped to produce. The DLL initial speed HS in the 2.54 cm gage length of the 6.35 cm specimen effective-length between grips was changed by load-train softness to 0.0127 m/min. It was further changed by HS skewing due to temperature. We say more about skewing in the DISCUSSION section.

The DLL e-t_L path to the N-path in Fig. 3b is representative of the curves of Fig. 4 where the DLL (elastic strain) path with the constant dead-load (transient strain) path leads to the CT N-path. The CT N-path is a constant-load isotherm that defines the CT curves in Fig. 4. N-points are points on a CT N-path. The total strain e at N on the CT N-path consists of the total DLL strain (the sum of elastic strain $e_O(L_O)$ and the transient, primary-creep strain e_{VE}). Recalling Fig. 3b, we saw that the position of any $N = N(L_O,T_O,e,t)$ on the CT N-path depends upon HS and t_L. t_L is the loading time to N from the start of loading to the tangent at N of the transient, primary-creep strain curve.

Upon extrapolation of the constant load CT N-path isotherms in Fig. 4, we found them to converge to the point $N_O = N(L_O,e_O,t_C)$ independent of the temperature. (We describe the compensation time $t_C = 34 \times 10^{-6}$ s further in the DISCUSSION section.) This convergence point is the incipient point N_O on a CT N-path independent of its temperature. It can, in principle, be produced with a DLL to Lo in $t_{LO} = t_C$ with an HS(MAX) at any convenient temperature.

Therefore, according to Fig. 4, upon "instantaneously" loading to N_O, the resulting curve is the CT N-path from $N_O = N(L_O, e_O,t_C)$ to $N = N(L_O,T_O,e,t) = Q$. This CT N-path is recognized as the primary creep curve envelope. This envelope is also the locus of the tangent points of the transient strains (which are also primary creep) due to all possible HS, $0 < HS \leq HS(MAX)$. Therefore, the DLL path can be manipulated to tangentially intercept any desired N-point on the N path, given the correct HS; that is, depending upon HS, the resulting transient, primary creep to N proceeds tangentially to a specific N-point on the CT N-path envelope which is the "instantaneously" loaded primary-creep path originating at N_O (for more, see the DISCUSSION section).

In Fig. 10 and its text, we will relate the concepts in the last three paragraphs to more familiar ones for creep loading.

As the SM-produced TMT curve stems from the same DLL method with the same HS as for the CT curve, it has its initial N-point on the CT N-path. Therefore, the TMT curve is LS equivalent to the CT curve at N; that is, N(TMT) = N(CT) = N(Lo,To,e), with the same loading time t_L.

To have CT-TMT LS equivalency at N, we recognized that a proper match between the $\dot{T}$ and the DLL HS is necessary. This implies that if apparatus is available for producing sets of heating temperature rates and DLL initial speeds, the relationship between these sets could be found by direct experiment. The experiment would yield the proper (undistorted) TMT curves from the proper HS-$\dot{T}$ matches. Even without this capability, the proper HS-$\dot{T}$ relation was obtained by comparing the temperature-skewed DLL initial speeds in Fig. 4 to heating temperature rates obtained from a procedure which produced a TMT curve with a non-constant, monotonically-decreasing $\dot{T}$ (not shown). From such a TMT curve, with a constant stress of 9.19 MPa, we matched selected $P(L_o,T_o,e,\tau)$ points to the $N(L_o,T_o,e,t_L)$ points in Fig. 4 as solid squares. The number beside each solid square in Fig. 4 indicates the $\dot{T}$ at N. It was then found, for example, that a $\dot{T}$ near 8 K/min matched an HS near 1.27 x 10-2 m/min (0.5 in/min). Fig. 8 shows the relationship of HS to $\dot{T}$ produced with the solid squares from Fig. 4. We outline the experiment in the DISCUSSION section.

The diagonal lines at 45° angles in Fig. 4 are constant strain rate and constant crosshead speed paths. They are designated "a" through "g". The strain rates increase by multiples of 10. At "a", the TT constant crosshead speed is 1.27×10^{-4} m/min with an associated strain rate of 2.8×10^{-5} s^{-1}, when the specimen initial length between grips is 7.62 cm and the effective length is 6.35 cm. At "g", the constant crosshead speed is 127 m/min with an associated strain rate of 28 s^{-1}.

From Reference 25, we superimposed the TT loading paths with constant crosshead speeds of 1.27×10^{-3} m/min (0.05 in/min), and 0.127 m/min--for HDPE in the uniform strain range--onto Fig. 4 in the e-t_L DLL plane. On each TT loading path, we indicated the stress level of 9.19 MPa along with a specific temperature, by hollow diamonds. For each temperature, the diamonds are connected by straight lines forming "isotherms" which are extrapolated, as dash lines, to shorter times. Then, these lines and their dash line extrapolations are constant load isotherms in the e-t plane. We called these constant load isotherms TT R-path isotherms (these R-paths are quasi-CT paths as they were derived by joining points of constant T_o and L_o on each TT loading path). With the same L_o and T_o, any TT loading path terminates at its respective R, on the R-path, and any CT/TMT DLL-path terminates at its respective N, on the N-path. At Q = $Q(L_o,T_o,e,t_L)$, denoted by solid diamonds in Fig. 4, there is an equivalence between the TT LS and time and the CT LS and time.

Since the R-paths and N-paths are intersecting straight lines at Q = N = R (on a log-log scale), it is apparent that no further LS equivalence is possible for N and R elsewhere. As this LS equivalence holds for only one HS-$\dot{T}$ combination, it is anomalous.

This anomalous LS equivalence holds provided the N and R points remain in the uniform strain region of the specimen. Therefore, uniform strain is a necessary condition for LS equivalence at Q, provided also that we subtract the thermal strain component from the strain of an N-point on a CT curve or a TMT curve before comparing the N-point to the corresponding R-point on a TT curve.

The R-paths and N-paths have unequal strain-time combinations everywhere except at their intersection at Q where there is LS and time equivalence. Although the intersection is described by equal values of load, temperature, strain, and loading time, the strain rates at Q for the R-path and N-path are not equal.

As an equivalence exists between the strains of the CT and TMT curves at Q, there is also an equivalence between the strains of the TT and TMT at Q. These LS equivalences originate from two separate loading methods which produce different loading paths.

Beyond 40°C the CT-TMT LS equivalence and the anomalous LS equivalence at Q fails. This is noticeable in the failure of the CT-TMT LS equivalence at 70°C and its position in Fig. 8. Exceeding uniform strain appears to be involved (this is corroborated in Fig. 6 where it is seen that the R-point is outside the uniform strain region at 70°C and 9.19 MPa).

Like the convergence of the N-paths to $N_0(L_0,e_0,t_c)$ the R-paths also appear to converge on further extrapolation. At this time, no significance is observed for this. Hence, the R-paths are extended only to the constant crosshead loading speed of 127 m/min (5000 in/min). WE take this speed arbitrarily as the constant crosshead-speed upper limit of the TT apparatus. This limit we marked with the appropriate load-temperature symbols (where the extrapolated R-paths intersect the arbitrary speed limit) in Fig. 4.

Strella (29) performed high speed loading (piston under gas pressure) on ASTM Type 1 HDPE specimens at a piston speed of 76.2 m/min (3000 in/min). He also performed a loading at 0.00254 m/min (0.1 in/min). He performed these tests at 23°C. From the Strella curves, at 9.19 MPa, we superimposed the strain for each piston speed on Fig. 4. We found these points from the Strella data to plot near the extrapolated 20°C R-path. As these tests are TT-type loadings performed at high and low loading speeds, they served as an independent check on the R-path and its extrapolation.

While the N-path from N_0 to Q is a creep-strain path in the e-t plane, recall that the position of a constant-L_0 transient-strain path and its tangent point at an N-point on the N-path depends upon HS. We can reach another N-point further up the CT N-path, however, after the N-point tangency occurs merely by waiting for the primary creep strain along the N-path to develop with time. Thus, there are optional DLL HS paths for arriving at a particular N. Take for example $N_2(L_0,T_0,e_2,t_{L2})$. N_2 may be reached directly at the end of the transient strain by using a proper HS, or N_2 may be reached indirectly by loading to N_1 and then using the N-path to N_2. That is, by first proceeding along a transient-strain path due to a particular DLL HS appropriate for reaching $N_1(L_0,T_0,e_1,t_{L1})$ (t_{L2} is greater than t_{L1} and the DLL strain rate to N_1

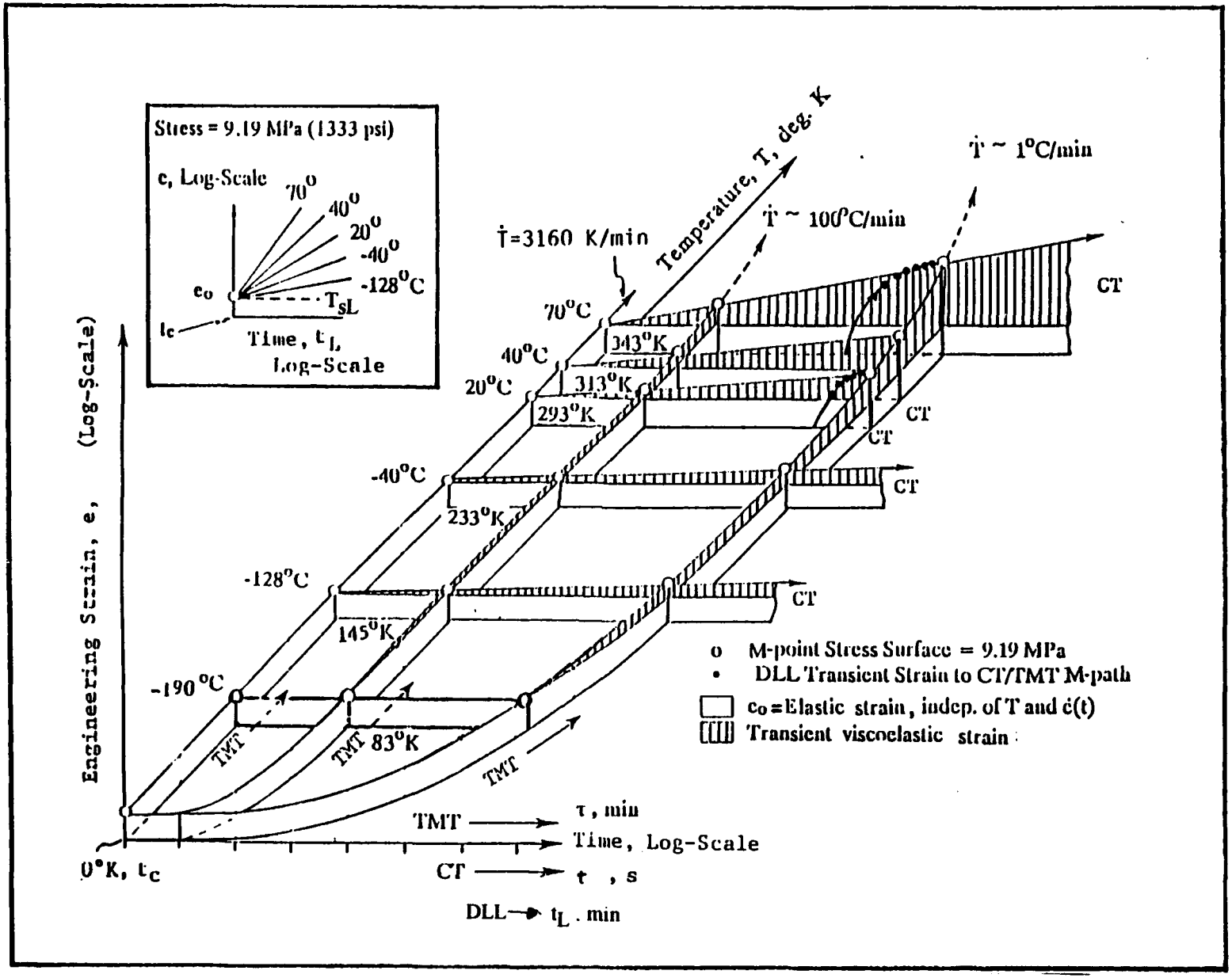

Fig. 5. Model for TMT-CT loading-strain equivalence in terms of a T-τ transformation for the TMT curves. The curves in Figs. 3a and 3b are its orthogonally projected components.

is faster than that to N_2) and then, after reaching N_1, proceeding along the N-path to N_2. The time t to N_2 along either path is the same, as seen in Fig. 3b.

The necessity to use the indirect DLL path to get to N_2 through N_1 occurred in Fig. 4. After the DLL of a specimen to an N, in t_L (near one second on the t-scale), with an HS of 1.27×10^{-2} m/min, Q was reached well along the CT N-path (nearly 30 seconds later on the t-scale). This need, again, was due to the experimental limitation of the single HS. Had the slower proper HS been available, the DLL of a specimen directly to N = Q in t_L (near 30 seconds on the t-scale) would have been possible. This correct HS is clearly achievable with a multi-speed DLL-mode apparatus.

Though experimentally limited to one HS in this paper, we see in Fig. 4 that an anomalous TT-CT LS equivalence exists at Q when exposed by an indirect DLL to any N, as the strain eventually leads to Q on the N-path. We avoid any such indirectness by a direct DLL (when available) to Q. This would result in a proper HS-$\dot{T}$ match with automatic TMT inclusion in the TT-CT-TMT LS equivalency (see the text of Fig. 8 for further details).

We can visualize apparatus for obtaining CT-TMT LS equivalent data over the complete testing range. This apparatus would posses a capacity for matching all heating temperature rates and DLL initial speeds. Fig. 5 is a model, depicting the CT-TMT LS equivalency produced with such apparatus over the complete testing range. For this paper, however, the model is theoretical beyond the present experimental testing range (that is, at the outer limits of HS and $\dot{T}$).

Fig. 5 is a schematic diagram of a constant load (stress) M-surface in 3-D "space" with coordinates of strain, temperature, and time. In the diagram we depict the CT-TMT LS equivalence connection from a DLL resulting in a common M. We may subsequently project M to N or P, as we stated in the text of Fig. 3.

Experimentally, TMT curves occur simultaneously in the e-T and the e-τ planes. The CT curve occurs in the e-t plane and DLL occurs in the e-t_L plane; Fig. 3 shows these. Combining curves in Figs. 3a and 3b results in the model in Fig. 5. We also based Fig. 5 upon Fig. 4 and relevant references. The model is useful for visualization of the relations of the e-t_L curves to the e-τ and the e-T curves and for the insights it contains on aspects of the loading problem. Refer to the texts of Figs. 3a and 3b and see the DISCUSSION section for conclusions based upon the loading model depicted by Figs. 3 and 5.

In Fig. 5, we ignore the thermal-strain component, along with the strain component due to w(i), as we did in Figs. 3a and 3b (establishment of the thermal strain requires a TDA scan over the complete T-interval $0\ K < T < T(Neck)$).

Above T_{sL} and with HS < HS(MAX), $e_0(L_0)$ and the transient, viscoelastic strain $e_{EV}(L_0,T_0,t_L\text{-}t_{L0})$ occur as components of the total loading-strain to $N(L_0,T_0,e,t_L)$. Fig. 4 suggests that $e_0(L_0)$ is dependent only upon L_0 above, as well as below, T_{sL}. Therefore, we

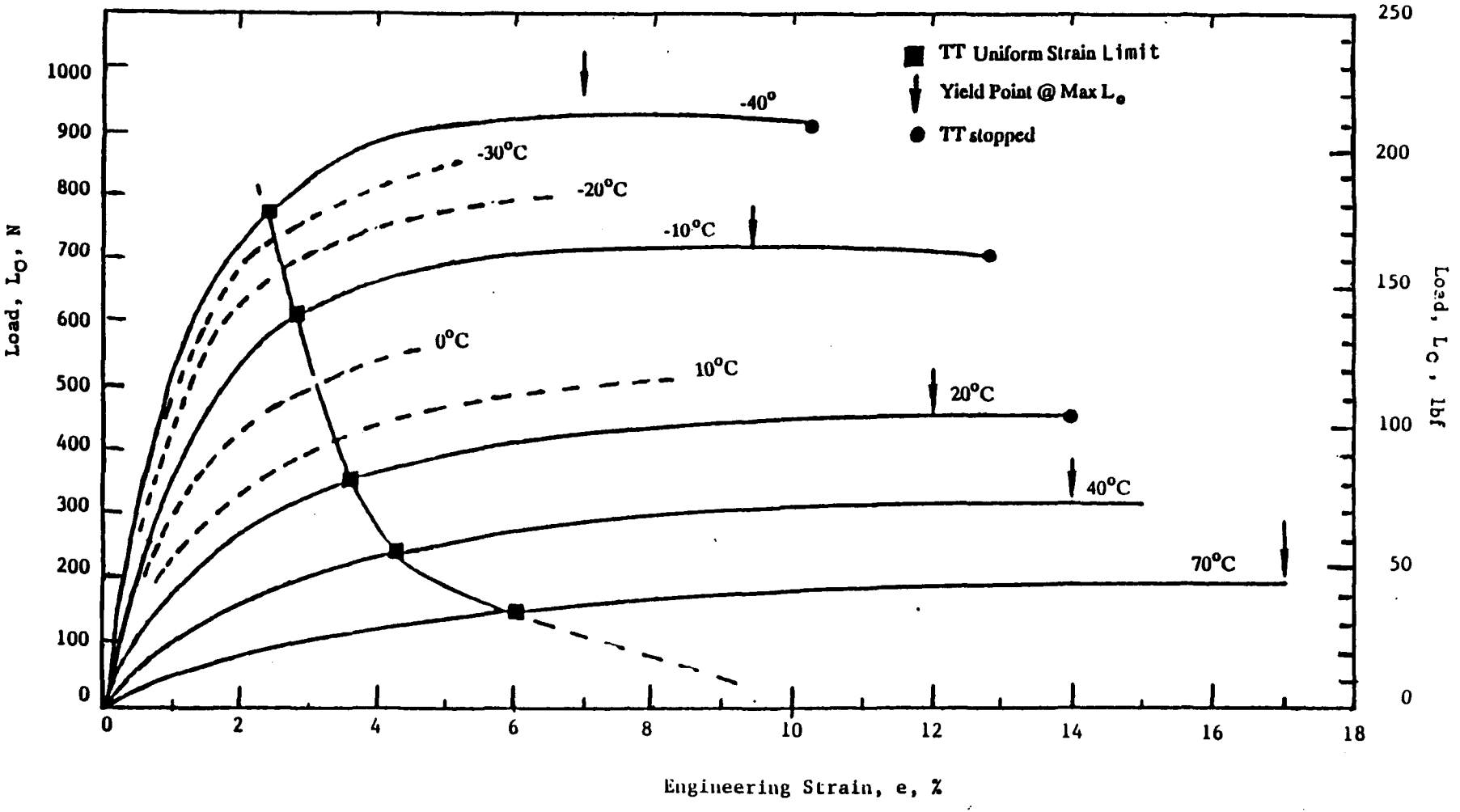

Fig. 6. HDPE TT data. Loading speed is 1.27×10^{-3} m/min (0.05 in/min).

show $e_o(L_o)$ separate from e_{VE} as a constant-strain component for all HS and all T, 0 K < T < T(Neck), in all the CT and TMT strains of the constant-load (stress) M surface.

Fig. 5 suggests that there is a set of constant-load M surfaces in the load range $0 < L_o < L_o(MAX)$ where $L_o(MAX)$ is the cutoff load for uniform strain in the specimen gage length; and, where L_o associated with 9.19 MPa produces a representative surface in this set.

Although any M on the constant-load (stress) surface in Fig. 5 is common to a TMT and a CT, due to common HS, the time t to reach a given M along the CT N-path is not equal to the time τ (both times reckoned from t_c) to reach it along the TMT-path. Of course, t_L is common to the CT and TMT during a DLL to M when the SM is used to produce a proper TMT curve with a proper HS-$\dot{T}$ match.

The inset diagram in Fig. 5 shows a set of isothermal creep-strain curves, with constant L_o and HS, like those in Fig. 4. Each creep curve, from a DLL with HS = HS(MAX), originates at $e_o(L_o)$ in t_c, independent of temperature. Each creep curve of the set in the inset may be considered an orthogonal projection from its own e-t plane onto a common e-t plane from its position in 3-D "space" as depicted in Fig. 5. Therefore, more generally, a set of creep curves occurs in 3-D space as shown in Fig. 5. In 3-D space, each constant load, CT N-path isotherm originates at $N_o = N(L_o,e_o,t_c)$ with its own temperature T_o in 3-D space. Therefore, we see any set of ubiquitous creep curves observed in the general literature as projections from 3-D space onto a common e-t plane.

TMT curves intersect CT N-path curves producing M-point CT-TMT LS equivalency at the intersections. All M-points on each CT isothermal curve will be intersected by a complete set of TMT curves and, conversely, each TMT curve will be intersected by the complete set of CT curves.

For each proper (undistorted) TMT curve, with a given $\dot{T}$, there is a correct HS producing a proper HS-$\dot{T}$ match. However, we must determine the proper HS-$\dot{T}$ pairing experimentally.

Fig. 6 contains TT curves of HDPE performed at the constant crosshead speed of 0.00127 m/min at the indicated test temperatures. The temperature is within ± 2°C. The dashed curves are interpolations. These TT curves are as the ones we refer to in Fig. 4 from Reference 25.

When we plot the TT data of Fig. 6 as e-T data in Fig. 7, we create a set of curves that resemble TMT curves. We will show these e-T curves to be undistorted TMT curves that we consider as though produced with a directly applied, correct HS somewhat greater than the TT crosshead speed of 0.00127 m/min to properly match $\dot{T}$ = 1 K/min at Q. (Recall the observed CT-TT anomalous equivalence due to an indirect DLL to Q in Fig. 4.). Until so shown in the text of Fig. 7, they will be tentative TMT curves constructed from the TT curves of Fig. 6 and we will designate them as TMT(TT) curves.

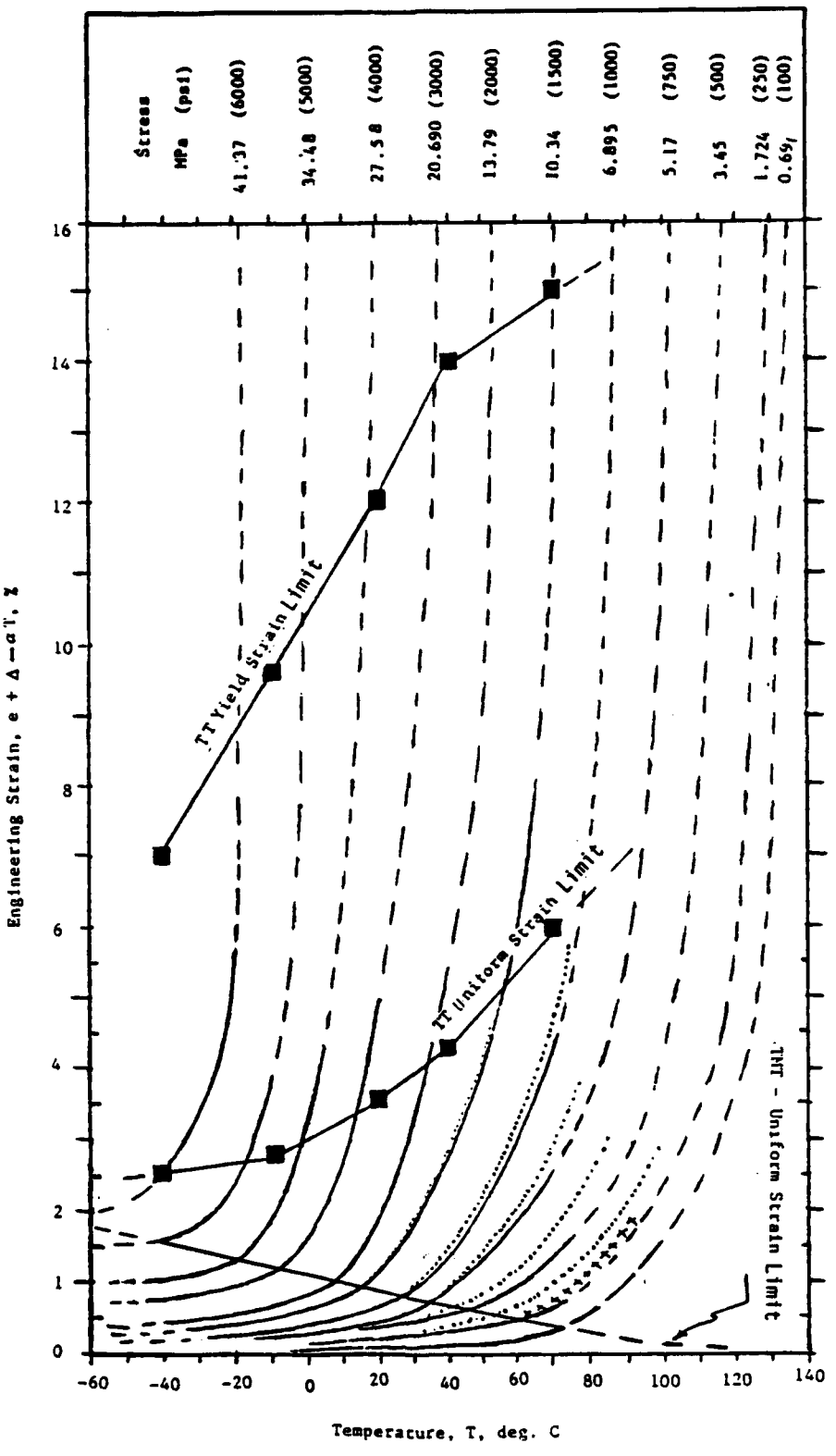

Fig. 7. TMT data produced from TT data in Fig. 6.

The TT curves of Fig. 6 are without thermal strain. The TT load is L_o = W(EX) where W(EX) takes on all values from zero to L_o. Correspondingly, the total strain for Figs. 6 and 7 is $(\Delta - \alpha To) + e[W(EX), To]$. When the thermal strain component of Eq. 1, shown in Fig. 1, is combined with the curves of Fig. 7, the result is a set of TMT(TT) curves as though produced with a $\dot{T}$ of 1 K/min and a correct HS. The exact value of HS is unknown, but is somewhat greater than the TT constant crosshead speed of 0.00127 m/min. (See also the text of Fig. 8.)

For a TT family of curves, between zero and the maximum load, we delineate three zones of strain by limits. These zones are the TMT uniform strain limit, the TT uniform strain limit, and the TT yield strain limit.

As used in this paper, for a given load (stress), uniform strain (also recall the text of Fig. 2) means all points in the volume of the gage length exhibit, on average, the same tensile strain; there is no severe local strain involved.

We superimposed on Fig. 7 the TT yield strains for the respective temperatures, obtained from Fig. 6 (arrows). They produce the TT yield strain limit.

We obtain the TMT uniform strain limit upon connecting the "knees" of the TMT(TT) curves in Fig. 7, at their points of maximum curvature (estimated). This limit defines the uniform strain range below which there is essentially negligible change in specimen cross section along the specimen effective-length in either the TT or TMT (or CT). It is the limit below which the TT and TMT (and CT) engineering stress-strain are essentially the same as the true stress-strain.

From Figs. 3a and 5, it appears that we may define the TMT softening point temperature, which decreases with decreasing $\dot{T}$ at constant dead-load, by the TMT uniform strain limit.

We consider the knee in any TMT curve to be a transitional point. From the present perspective, this point indicates the end of the TMT uniform strain and the start of the TT uniform strain in the gage length.

For comparison, we superimpose the TT uniform strain limit from Reference 25 onto Figs. 6 and 7; also onto Fig. 2. We obtained this TT uniform strain limit from a plot of specimen effective-length between grips versus gage length strain. We maintained each specimen at constant temperature during a TT (25). The TT uniform strain limit defines the strain where the specimen effective-length starts to decrease. The decrease in effective length indicates the start of an increasing strain rate in the gage length.

The segments of the e-T curves in Fig. 7, from -55°C up to the TT uniform strain limit, apply to the TMT as well as the TT: the undistorted TMT curves produced by means of the correct DLL initial speed (HS) and matched $\dot{T}$ would be congruent with these TT segments in the TT uniform strain range. In the TT uniform strain region, the TMT and TT strain is uniform in the gage length as the cross section decreases uniformly. Beyond this range, into the necking

range, there is significant TMT curve deviation. This is because the TMT carries its dead-load throughout the test while the TT adjusts its load to accommodate the changes in specimen cross section.

Apparently, the condition of uniform strain, common to the TT and TMT up to the TT uniform strain limit, is a requisite for TT-TMT LS equivalence at $Q(L_O,T_O,e)$; the other condition is that the HS match $\dot{T}$ in the TMT curve. If the transient DLL path is to intersect the TT loading path at Q, the correct HS for the HS-$\dot{T}$ match needs to be somewhat larger than the TT crosshead speed of 0.00127 m/min. The matching requirement for a proper TMT, along with the condition of uniform strain for both the TT and TMT, is the necessary and sufficient conditions for TT-TMT LS equivalence at Q (recall the text of Fig. 4 and see Fig. 8 for other details on Q-point equivalence).

To compare the TMT(TT) curves of Fig. 7 to the TMT curves of Fig. 2, we added the thermal strains, with $\alpha = 74 \times 10^{-6}\ K^{-1}$ and $110 \times 10^{-6}\ K^{-1}$, in turn to each TMT(TT) curve of Fig. 7. We plotted the two sets of TMT(TT) curves of Fig. 7, differing by the thermal strains resulting from the two values of α, on the TMT curves of Fig. 2. The solid circles belong to the total TMT(TT) strain with $\alpha = 110 \times 10^{-6}\ K^{-1}$. These satisfy congruence best between the data of Figs. 2 and 7 in the TT uniform strain region. We discussed a reason for lack of full congruence of Fig. 2 TMT curves with the TMT(TT) curves of Fig. 7 in the texts of Figs. 2 and 3.

Note that the loading time to Q for the TT is the same as that for the CT or TMT. Note also that we refer all TT loadings, to any R, to the e-t_L loading plane used for CT-TMT DLL to any N.

Let us summarize the experimental results used to show LS equivalence between TT, CT, and TMT at Q as follows:

We found the CT in Fig. 4 and the TT in Fig. 7 equivalent at Q.

We constructed the TMT(TT) curves in Fig. 7 from TT curves in Fig. 6.

Therefore, the TMT(TT) strain of Fig. 7 equivalently fitted the CT strain of Fig. 4 at Q.

From the partial congruence of the Fig. 7 TMT(TT) to the Fig. 2 TMT, we deduced the correct $\dot{T}$ required for the proper TMT(TT) of Fig. 7 that matched an HS somewhat larger than the HS = 0.00127 m/min as follows: when a mismatch between HS and $\dot{T}$ occurs in the synchronization maneuver region, a distorted TMT curve is produced. This was the case with the TMT curves of Fig. 2. There was a mismatch between the HS of 0.0127 m/min and the $\dot{T}$ of 1 K/min. The higher the loading speed, the lower the strain to N (see Fig. 4). As a result, the TMT curves of Fig. 2 are lower in strain than the corresponding TMT(TT) curves of Fig. 7 at the low temperature loading end.

After loading for a TMT, the dominant effect on strain beside Lo is the temperature. Under a constant $\dot{T}$ of 1 K/min, the Fig. 2 TMT curves tend to the TMT(TT) curves of Fig. 7 as the temperature increases. Both sets become congruent at the high temperature end. Then the constant $\dot{T}$ of 1 K/min appears to be common to both sets of curves. Therefore, the $\dot{T}$ best suited for the Fig. 7 TMT(TT) is that of the Fig. 2 TMT curves. Therefore, the Fig. 7 TMT(TT) curves are undistorted TMT curves with an unknown HS somewhat larger than 0.00127 m/min and a matching $\dot{T}$ of 1 K/min, as stated in the text of Fig. 8.

Further, we expect any TMT(TT) curve in Fig. 7, although constructed from the TT curves of Fig. 6, to have an existence of its own as a TMT curve. That is, we expect it to be experimentally producible on its own, given the correct HS near 0.00127 m/min and a matching $\dot{T}$ of 1 K/min. Such a set of TMT curves could then produce an equivalent set of TT curves at Q

Furthermore, the existence of the anomalous equivalence is the reason that the set of TMT(TT) curves of Fig. 7 was constructible from the TT curves of Fig. 6. At $N < Q$, no other set is constructible this way--precisely because the relation is anomalous--nor can the TMT curves at any $N < Q$ construct an experimentally verifiable TT family.

In Fig. 4, the CT-TT LS equivalence at Q, for the stress of 9.19 MPa, is only for a slice through the Fig. 6 TT set of curves. However, because the CT is LS equivalent to the TMT for all N over the L_o-T_o milieu in the TT uniform strain range, the CT is LS equivalent to the TT at Q for all stress and temperature combinations producing strains in the TT uniform strain range. Therefore, Fig. 7 (or Fig. 6) represents the anomalous TT-CT-TMT LS equivalence in the e-t_L plane over the whole L_o-T_o milieu in the TT uniform strain range.

Due to systematic errors in the DLL and TT loading modes, there is a strain difference between the TMT curves of Figs. 2 and 7 above 20°C. The size of this strain error is given by the strain difference between the 0.69 MPa TMT e-T curves of Figs. 2 and 7. Superimposing the one from Fig. 2 onto Fig. 7, we show that the error or strain difference between these 0.69 MPa curves is proportional to the temperature. Due to consistent experimental technique, this strain difference, at the same T_o, is the same for each curve of the set of e-t curves in Fig. 7. We found that this strain difference is 0.4% at 70°C, decreasing to about 0.11% at 20°C. Then, if we adjust the TT e-T curve of stress 0.69 MPa in Fig. 7 by adding these strain differences to it, it becomes congruent with the 0.69 MPa TMT e-T curve of Fig. 2. Likewise, we adjusted the other curves in Fig. 7 between 0.69 MPa and 13.8 MPa for stress. WE show these as dotted lines. Above 13.8 MPa and below 20°C, the adjustments are negligible within the TT uniform strain region. We did not incorporate these strain changes into the solid and hollow circles superimposed on Fig. 2.

We will see from Fig. 8, that we require a $\dot{T}$ greater than 1 K/min (about 4 K/min) matched to the HS of 0.00127 m/min. This is necessary for the replacement of the curves in Fig. 2 with undistorted TMT curves. There would then be a proper match for a CT-TMT LS equivalence, but these replacement curves would not belong to the set of TMT curves, with a $\dot{T}$

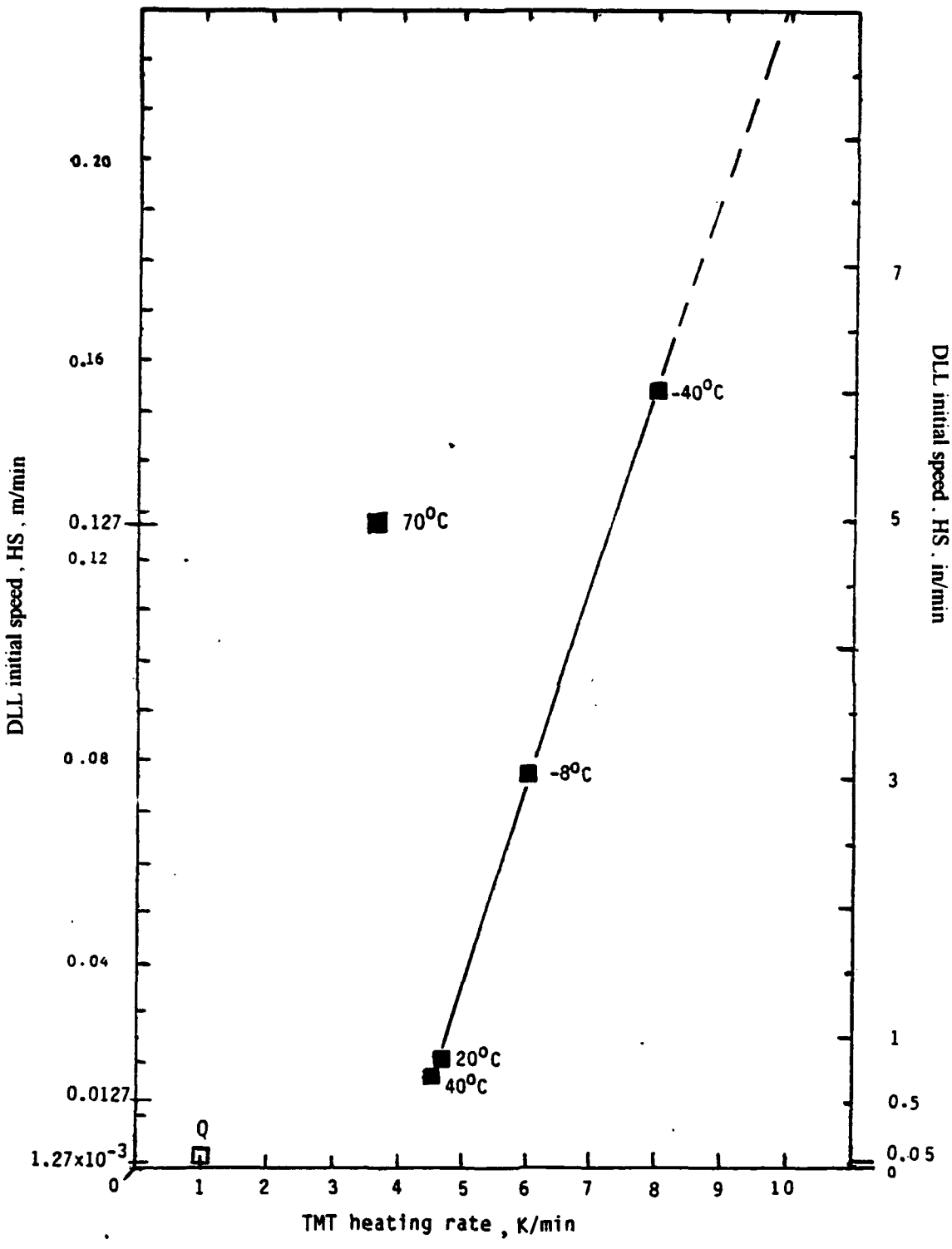

Fig. 8. HS-$\dot{T}$ relationship for HDPE indicating TMT-CT loading-strain equivalence when strain is below the TT uniform strain limit.

of 1 K/min, that are anomalously LS equivalent to the set of TT curves produced with the constant crosshead speed of 0.00127 m/min.

Fig. 8 relates the crosshead speed and DLL HS to the TMT $\dot{T}$ at N. We present here three LS equivalence conditions and their relation to Fig. 8. They are the CT-TMT LS equivalence condition, the anomalous CT-TMT-TT LS equivalence condition, and the loading condition with intrinsic w(i).

The first condition involves loading and temperature as presented in Fig. 3 for a TMT curve but with a nonconstant $\dot{T}$ (not shown, but we describe its production in the DISCUSSION section). For specimens loaded at -55°C with HS = 0.0127 m/min, with a stress of 9.19 MPa, we obtained the strains and heating temperature rates directly at 40°C, 20°C, -8°C, and -40°C. We superimposed this data as solid squares on the N-path strains at temperatures corresponding to the isotherms in Fig. 4. Then, the DLL initial elevator speeds (HS), deduced from the temperature skewed DLL initial strain rates of Fig. 4 (shown as dotted lines of slope 45° tangent to the skewed DLL curves), are plotted against the corresponding heating temperature rates to produce Fig. 8 (see the DISCUSSION section for experimental details).

Thus, we produced a quantitative relation between HS and $\dot{T}$. This relation defines the HS - $\dot{T}$ combination for a proper HS-$\dot{T}$ match which is required to obtain undistorted curves for CT-TMT LS equivalence. We expect the relation to hold over that part of the constant stress M-field in Fig. 5 that is within the TT uniform strain limit.

The position of the solid square at 70°C in Fig. 8 indicates that it does not belong to the relations of Fig. 8. The data appears to be outside the TT uniform strain limit (recall the texts of Figs. 4, 6, and 7).

The second loading condition occurs at $Q(L_O,T_O,e)$ and deals with the anomalous TT-TMT-CT LS equivalence for a single HS-$\dot{T}$ pair within which the TMT-CT LS equivalence is valid with this same, single HS-$\dot{T}$ pairing.

Although the HS required for a direct DLL to Q (recall Fig. 4 text) was experimentally unavailable, it is, nevertheless, seen that the TT R-point and CT N-point are LS equivalent at Q. Then the TMT N-point is also equivalent to the R-point at Q. This is the anomalous TT-CT-TMT LS equivalence described in the text of Fig. 7.

We made the anomalous TT-CT-TMT LS equivalence at Q with two loading modes: the CT-TMT LS equivalence at N = Q originating from the DLL mode, and the R-point at Q originating from the TT loading. The TT loading path to Q occurs at a constant crosshead speed (0.00127 m/min) while the CT-TMT DLL-path starts with a direct HS somewhat greater than the TT speed resulting in a transient viscoelastic DLL path which intersects the TT path at Q. Therefore, inherently the DLL and the TT loading paths to Q are different and consequently there is an irreconcilable speed difference between the TMT HS direct to Q and the TT crosshead

speed. If we knew this TMT HS, we could plot the HS-$\dot{T}$ point at Q in Fig. 8, but it would not represent the TT loading speed. Therefore, the anomalous TT-CT-TMT LS equivalence does not have a unique HS-$\dot{T}$ point in Fig. 8. Although there is no unique HS-$\dot{T}$ point for the anomalous TT-CT-TMT LS equivalence at Q, we can, however, plot it tentatively with an HS slightly larger than the TT speed of 0.00127 m/min as a hollow square and designate it Q in Fig. 8. The CT-TMT portion of the anomalous LS equivalence has a proper HS-$\dot{T}$ match at Q independent of its anomalous TT LS equivalence. This portion is CT-TMT LS equivalent.

The third condition, with the intrinsic load w(i), does not have an explicit HS. Therefore, the loading of a specimen with w(i) precludes the use of the SM. This condition involves Fig. 1 and the solid squares superimposed on it. We took these solid squares from the nonconstant-$\dot{T}$, TMT curve made with L_o = w(i) and, like Δ of Fig. 1, of unknown HS (with this nonconstant-$\dot{T}$ curve we produced a set of heating temperature rates similar to the way we produced the set for the 9.19 MPa mentioned above and with loading described in the DISCUSSION section). Each $\dot{T}$ of the set occurred at a specific temperature. This set, as well as that produced with the 9.19 MPa loading, was governed by the initial $\dot{T}$ generated by the momentary conditions existing in the EC at the start of the TMT at -55°C (see the DISCUSSION section for further experimental details). We plotted these heating temperature rates at their temperatures as solid squares in Fig. 1. The numbers beside the solid squares are the nonconstant heating temperature rates in K/min.

Fig. 1 indicates that any P (or N) of Δ is independent of $\dot{T}$. This is corroborated by the position of the solid squares in Fig. 1. Therefore, for the third condition, there is no unique match between HS and $\dot{T}$, but, if we knew the HS for a DLL to w(i), we could represent the condition of a TMT independent of $\dot{T}$ by a line HS = C in Fig. 8.

Fig. 9 is a plot of Troutonian viscosity versus temperature at constant dead-load (or constant stress) below the melting temperature of HDPE (140°C).

The Troutonian (or extensional) viscosity at P (or N) on a TMT curve in the e-T plane is given by

$$\eta_{ex} = \text{stress} / [e'\dot{T}] \qquad \text{Equation 3a}$$

or

$$\eta_{ex} = \text{stress} / \dot{e} \qquad \text{Equation 3b}$$

where $\eta_{ex} = 3\,\eta$(Newtonian).

Eqs. 3a and 3b, along with Eqs. 2a and 2b, are used to indicate how the T-τ transformation works, by the example here of plotting the extensional viscosity of HDPE as a function of temperature for two engineering stress levels.

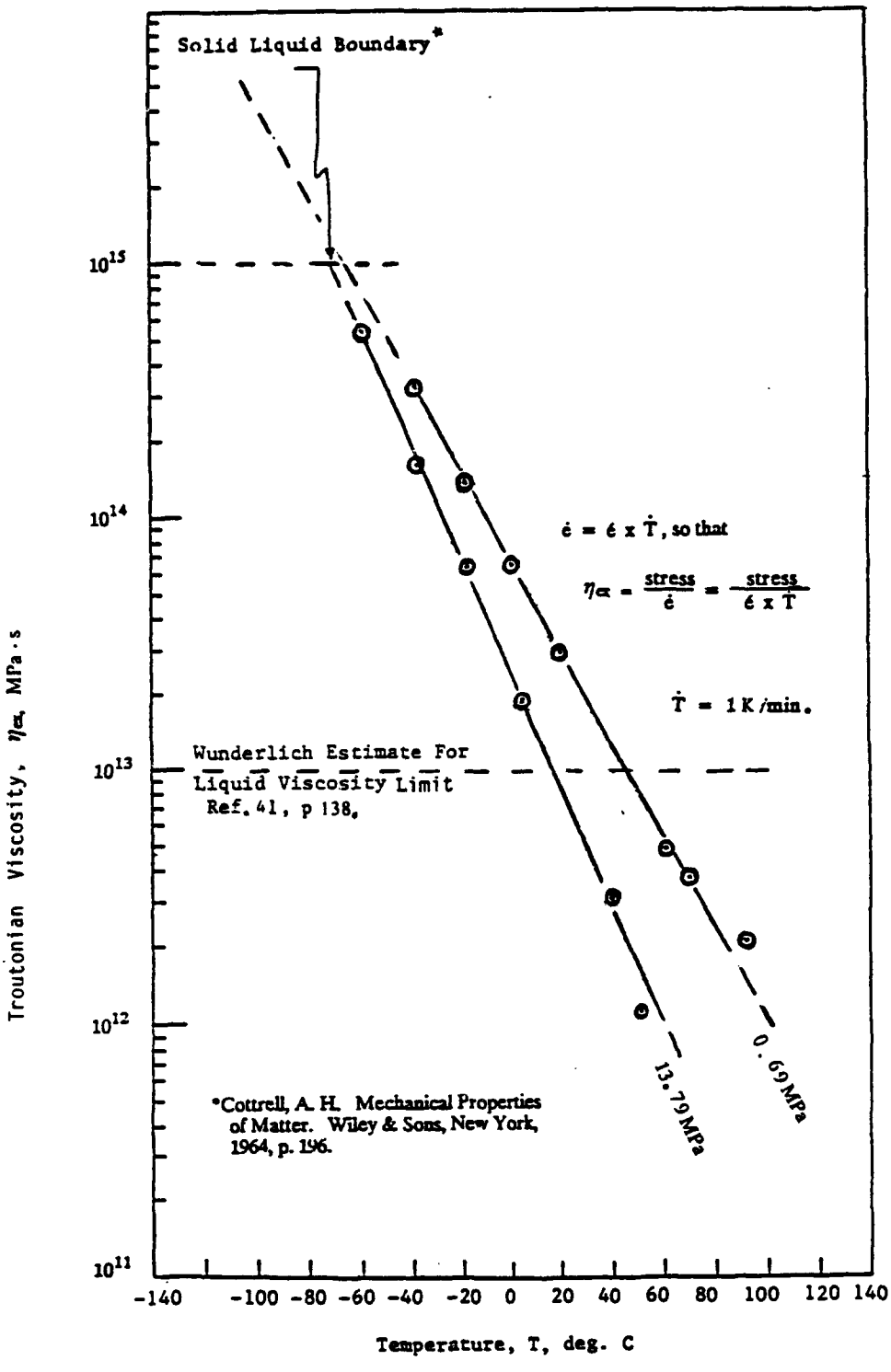

Fig. 9. Trotonian viscosity as a function of of temperature from the data of Fig. 7 at two stress levels.

We obtained the data for Fig. 9 from two curves of the TMT curve-set of Fig. 7 (this data is in the anomalous LS equivalence Q region). These TMT curves are without the thermal strain component. Tangents to these TMT curves produced sets of slopes for several loads. We took these slopes to represent e' = de / dT in Eq. 2b. Using Eq. 2b, we then substituted results into Eq. 3a--along with the heating temperature rate of 1 K/min--to obtain η_{ex} at selected temperatures. Plots of the log of η_{ex} versus temperature produced straight lines of constant load or stress. These lines show that the extensional viscosity decreases along a TMT curve (of constant load or stress) with increasing temperature, or increasing TMT strain-rate $\dot{e}$; while at constant temperature, the viscosity decreases as the stress increases (apparently due to a faster strain rate increase than the stress increase)

As the method for obtaining the two lines was primitive, we expect that the results are approximate. Computer techniques--whereby the computer samples real-time e-T data and then calculates e'(at constant stress and T)--would produce more accurate results for η_{ex} with these variables.

If the thermal strain component αT_0 is included, a different set of curves, shifted slightly to lower viscosity, would result.

Strain rate is a dominant feature of Troutonian viscosity. As this viscosity depends upon strain rate, its direct outcome at any N or R depends on the strain rate at these points. We consider several extensional viscosities at N (and R) due to the strain rates involved in the TMT and the CT (and the TT).

Although the TMT and CT curves have the same DLL path to a common N in the e-t_L loading plane, they do not have equal strain rates at this N --or any other N-- when two such curves intersect as a result of the superposition of e-τ and e-t planes as in Figs. 3b and 5 (completely removed from the SM-application region). This includes N = Q (recall Figs. 3, 4, and 5).

Therefore, the extensional viscosity for a TMT point at any N reached by a DLL is equal to that for a CT point as they use the same DLL to this N (where the CT and TMT paths initiate) because de / dt_L is the same. Note that this is the SM application point producing a discontinuity in the TMT curves.

But when a TMT and a CT curve intersect in the superposed e-τ and e-t planes, $\dot{e}$ > de / dt (where de / dt is the CT N-path strain rate). Thus, although the two planes use different time scales we can easily get a relative comparison of viscosities for the TMT and CT curves at any N.

At Q, the CT N-path strain rate is greater than the TT R-path strain rate (recall Fig. 4). Therefore, the extensional viscosity at N = Q on the CT N-path is less than that at R = Q on the TT R-path, while that of the TMT N-path at Q is less than either. Also at Q, reached in a time t_L, the extensional viscosity from a TT loading-path strain rate to Q is less than the extensional viscosity at Q from the TT R-path strain rate.

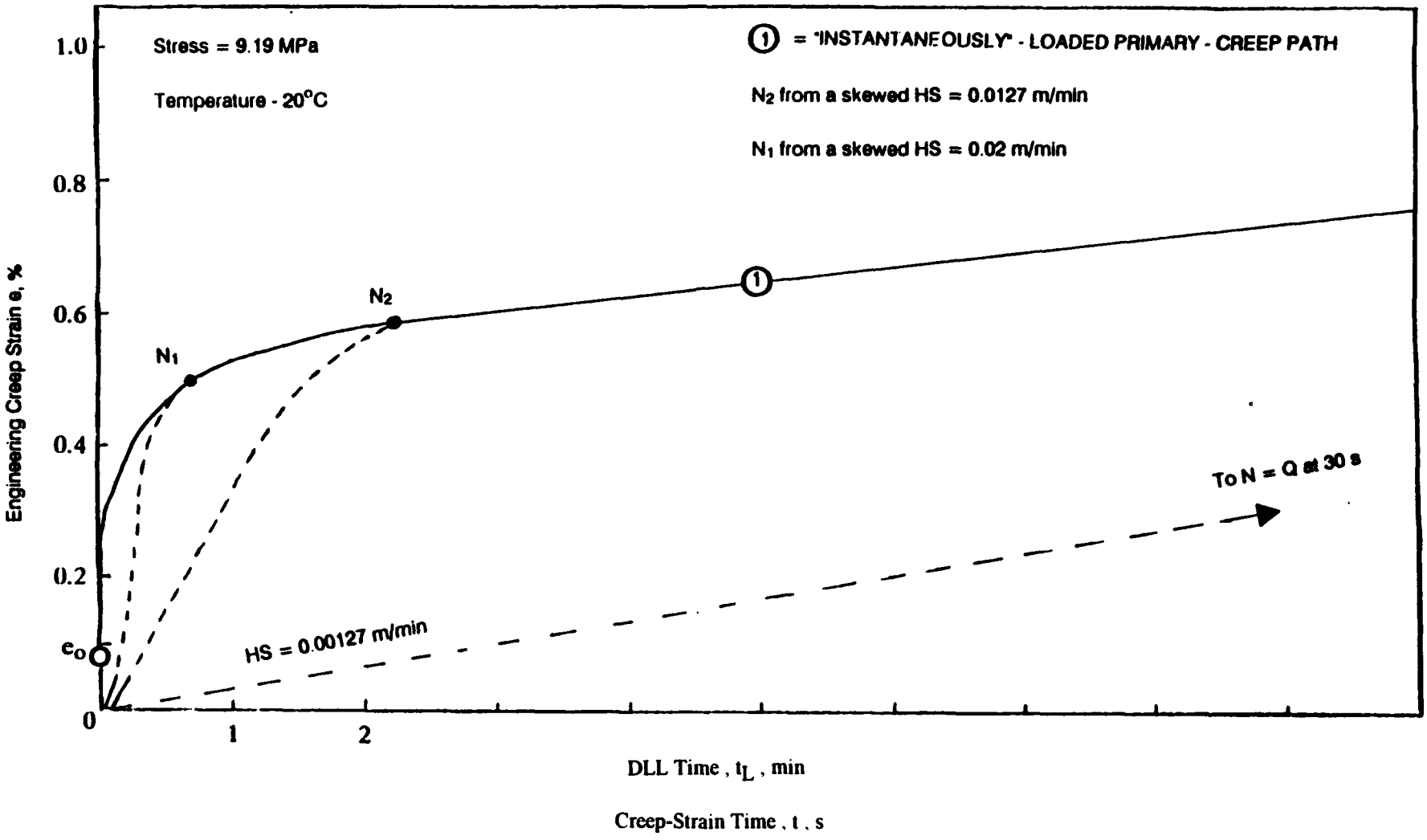

Fig. 10. A 20°C CT N-path in linear coordinates: a representative curve from Fig. 4 showing loading paths to the N-path with several dead-load loading rates.

Likewise, the extensional viscosity of the TT strains differs from that of the equivalent TMT loading strains in Fig. 7 (at N = R = Q) because the TT loading strain-rate is greater than that of the TMT DLL initial strain-rate at the equivalent TT-TMT strain.

These considerations indicate that we can know the TMT and CT Troutonian viscosities--on a relative basis in this paper--at any M on a constant stress surface (recall Figs. 3 and 5). The Troutonian viscosity, in the e-τ plane, along the constant load, constant $\dot{T}$, TMT curve (recall Fig. 3b) decreases with increasing τ_O, T_O, and $\dot{e}$; while the viscosity increases with decreasing strain rate de / dt along the constant load, constant temperature CT N-path; that is, along a primary creep curve in the region exhibiting uniform creep strain. We do not consider Troutonian viscosity in this paper for nonuniform strain.

Fig. 10 sets the N-path CT curves of Fig. 4 in a familiar framework and terminology by presenting the 20°C isotherm replotted on a linear e-t graph. This 20°C isotherm--representative of the other isotherms of Fig. 4--is a CT N-path curve with the limits $N_O \leq N \leq Q$. Such an isothermal, CT N-path can result from an "instantaneous" DLL with L_O and HS(MAX) to $N_O = N(L_O,e_O) = e_O(L_O)$ in $t_{LO} = t_c$ for any and all $T_O \geq T_{sL}$.

We consider that an isothermal, CT N-path--starting at N_O and ending at Q--is a primary-creep-curve envelope. Therefore, any DLL path--with L_O and HS(at Q) $\leq$ HS < HS(MAX)--which tangentially intercepts the N-path envelope at N from below, will produce an isothermal, primary-creep curve (at the same T_O as the CT N-path envelope) congruent with the N-path envelope. The tangent point depends upon HS.

Looking at the CT-TMT LS equivalence relationship, we see that the M (or N or P) points on a TMT curve consist of points from a set of primary creep-strain curves. Then, in Fig. 5, the TMT curves consist of equivalent primary-creep strain. The two sets of curves, with LS equivalence, intersect at all M points. Each curve of an intersecting curve-pair of TMT-CT LS-equivalent curves, however, has its own strain rate at M caused by and propagated by its characteristic energy source. The source for the decreasing transient strain rate along a primary creep curve is a constant T_O and a constant L_O; and the source for the TMT curve with increasing strain rate is a constant $\dot{T}$ and L_O.

Note that the TT strain at Q, which is equivalent to the total creep strain at Q, is a forced loading strain in phase with the load. Likewise, for a CT, the elastic strain component is in phase with the DLL to $e_O(L_O)$, while the transient primary creep strain leading to Q occurs under constant L_O and a decreasing strain rate.

Therefore, the anomalous CT-TMT-TT LS equivalence involves three intersecting curves. Each curve is propagated by its own characteristic energy to a common LS point $Q(L_O,T_O,e)$. This is why the TMT(TT) curves, produced in Fig. 7 from Fig. 6, did not have a $\dot{T}$ or HS directly attributable to them. We deduced $\dot{T}$ and HS for the TM(TT) curves from other sources (recall the text of Fig. 7).

Note that we did not develop the experimental curves in Fig. 4 sufficiently beyond Q to fix the end-point of primary creep.

DISCUSSION

With due regard to the manner of loading of a HDPE specimen, we found that CT-TMT LS equivalency is dependent on the loading method and the proper HS-$\dot{T}$ matching, as well as load and temperature.

We attempted to answer questions such as:

Is the TT loading method related to the DLL method and if so, how?

Is the CT related to any other mechanical test besides its anomalous LS equivalence relation to the TT?

What are the prime requirements for CT-TMT LS equivalence?

Where does DLL end and the CT path and TMT path begin? Is HS involved and if so, how? How is the $\dot{T}$ involved?

What is the relation of the TMT curve to the CT curve after they both emanate from the same DLL curve at N?

These are some of the questions involved in what we call the "loading problem".

Mechanical loading (like DLL and TT loading) and its effect on the CT and TMT -- particularly for plastics susceptible to large deformation under relatively small loads-- is a problem because of the resulting confusion in comparing data from diverse sources without knowledge of how this diversity affects a test and its relation to other tests. This is due to the acceptance by many of using arbitrary loading methods for initiating a mechanical test, without any consideration of loading rates or heating temperature rates in many cases. Indeed, almost all loading methods -- for almost any type of mechanical test-- appear to be under the sway of arbitrary loading. In most cases, as exemplified by a case for metals, creep loading and its effects are ignored (30) (although this may be true for metals under certain conditions, this is not so for plastics as exemplified by HDPE in this paper), and in many cases it is believed that loading does not affect the mechanical test it initiates. A common example of this is the arbitrary procedure, for example, as used in Reference 31, which omits the loading portion of the test when presenting experimental data. In some cases, again arbitrarily, the experimentalists omit the loading strain deliberately because it appears complicated for inclusion, being perceived correctly as related not only to loading and heating temperature rates but to the specimen's geometry and the apparatus (32).

The task in this paper was to determine which perceptions about loading are valid at least for some plastics, although the general problem of loading appears to hold for all materials.

Figs. 3, 4 and 5, combined, are a model representing two cases: CASE 1 is the model where the TMT(e-τ) plane containing TMT curves is superimposed on the CT(e-t) plane cotaining CT curves. In CASE 2 each curve is made of a series of M-points, each from a different DLL HS. It is represented by the e-t_L plane in Figs. 3b, 4 and 5 wherein the e-t_L loading plane is superimposed on the planes of CASE 1. An N-point from CASE I will have a LS equivalent N-point in CASE II. Thus, a loading with the SM involves using both cases: CASE II for loading and CASE II for the resulting TMT/CT curves. Note that TT loadings also use the e-t_L plane.

In review, according to Figs. 3, 4 and 5, the loading method and the loading rate affect the position of N on the TMT and CT curves, and of R on the TT curve and, therefore, the subsequent relationships of R and N for HDPE. The DLL method appears to be the prime mechanical loading method for initiating an N-path CT or TMT. For an HDPE specimen under a DLL for a CT or TMT, the mechanical loading problem deals with the specimen response to a DLL and with the subsequent position of N on the N-path. The initial specimen response to the DLL occurs during the elastic loading strain that is completed when the loading reaches the full load L_O. Then, the full load imparted by the DLL produces a transient-strain response up to N = $N(L_O,T_O,e)$. This point is common for the CT and TMT. At this N, the loading problem further involves the proper matching of the HS to the TMT $\dot{T}$ for a CT-TMT LS equivalence. The strain at this N denotes the response to the DLL as the sum of elastic and transient (primary creep) strain to t_L. Then, the full dead-load, acting upon the specimen at N, is transferred from its action on the DLL transient strain (with the SM) to produce TMT strain or to continue undisturbed from this N on the N-path as primary creep strain. The resulting TMT and CT curves are congruent with any corresponding N-path curves produced earlier with faster DLL HS's.

When the position of N in the e-t_L plane is due to the DLL HS, then, the CT and TMT strain rates are equal at N (CASE 2). In Figs. 3 and 5 (CASE 1), we obtained the CT strain rate at N on the N-path from the strain e and t at N, while the TMT strain rate at N (see Eq. 2b), on the TMT N-path, depends upon e and τ. The CT and TMT N-path curves approach and intersect at $N(L_O,T_O,e,\tau_O,t)$. From N they continue along separate N-paths with their own strains and strain rates; that is, on the t-scale for the CT and the τ-scale for the TMT. Each curve from either the CT or TMT set, however, intersects all curves on the other set in the constant stress M field (recall Figs. 3 and 5).

A curve production requiring the SM is a segment of a whole TMT curve produced at its high temperature end. To produce a whole TMT curve starting at $N(L_O,T_O,e,t_L,\tau_O$ with the DLL method requires, once again, the use of the SM. A whole, or complete, TMT curve starts at $N_{sL} = N(L_O,T_{sL},e_O,\tau_{sL})$ and contains both the elastic and the viscoelastic strain.

We omit the thermal strain component from consideration in most treatments in this paper. We subtracted it from the Δ-adjusted total strain in Figs. 3, 4, and 5.

We propose and will show that the curves in Figs. 3 and 5, though theoretical and unverified in this paper when extended to extremes of temperature, time, HS and $\dot{T}$, present a consistent and complete DLL strain model. The treatment follows.

Using the model described in the texts of Figs. 3 and 5, the data of Fig. 4, and other relevant references, we will now show for HDPE how a DLL at the TMT-curve loading-source point $N_S = N(L_O,T_S,e_O,\tau_S)$ with the aid of the SM might produce a whole TMT curve over the whole temperature range $0\ K < T < T(Neck)$ (compare to Fig. 3a). The temperature intervals $0\ K < T_S \leq T_{SL}$ and $T_{SL} < T_O < T(Neck)$ comprise the interval $0\ K < T < T(Neck)$. The associated τ-time intervals is $t_C \leq \tau_S \leq \tau_{SL} < \tau_O$. Further, although the SM and a proper HS-$\dot{T}$ is still required when the TMT is loaded and initiated at $T_S < T_{SL}$, the advantage is the production of the whole TMT curve. A TMT curve ends when its strain reaches the TT uniform-strain limit (incipient necking). τ_S and T_S are the TMT-curve, loading-source time and temperature in the time interval $t_C \leq \tau_S \leq \tau_{SL}$ and the temperature interval $0\ K \leq T_S \leq T_{SL}$. Together they comprise the T_S-τ_S loading-source region for a CT curve or whole TMT curve production at N_S. T_S and τ_S are related by Eq. 2a.

In the T_S-τ_S region, we first generate the strain at an N_S-point (which designates the starting point of an elastic-strain-only CT curve or an elastic-strain-only TMT curve followed by whole TMT curve) by a DLL in the loading time t_{LO} to $N_S = N(L_O,T_S,e_O,HS[t_{LO}])$--where $t_{LO} \geq t_C$ ($t_C = 34 \times 10^{-6}$ s) is the range of loading times for DLL in the e-t_L plane. Recall that these loading times are associated with the DLL initial speed range $HS \leq HS(MAX)$. From the e-t_L plane, we may then project this point as the start of an elastic-strain-only CT or TMT curve onto the T_S-τ_S region. The production of an elastic-strain-only TMT curve in the T_S-τ_S region, however, requires (by CASE 1 above) that the N (resulting from a DLL in the e-t_L plane be plotted in the e-τ_S plane. Then in the e-τ_S plane, $N_S = N(L_O,T_S,e_O,HS[\tau_S])$. The CT in this region proceeds as an isotherm at constant L_O along the T_S-ordinate from the incipient N_S in the e-t plane at a constant strain $e_O(L_O)$. This CT-path intersects the elastic-strain-only TMT curve initiated at the same N_S.

It is through $N_O = N_S = N(L_O,T_S,e_O,t_C)$, from Fig. 4 and relevant references, that we set the theoretical limits of Figs. 3 and 5 which we will now attempt to develop and use.

In Fig. 4, we see that with decreasing temperature the CT N-path isotherms (the constant load and constant temperature primary creep curves) appear to approach the limiting strain of the point N_O. Fig. 4 suggests that N_O exists, independent of temperature, in the temperature interval somewhere below 145 K (herein called the T_S-t_L loading-source range). The HDPE data of Reference 33 indicates that the limiting strain of the N_O-point is the constant elastic strain $e_O(L_O) = C$ for all CT N-path isotherms in the interval $0\ K < T_S \leq T_{SL}$ where $T_{SL} = 83$ K is the upper limit of the temperature interval for the strains described by $N_S = N(L_O,T_S,e_O,t_L)$. The time interval $t_L \geq t_C$ is in the T_S-t_L loading-source range in the e-t_L plane.

The modulus obtained with $e_O(L_O)$---at $N_O = N_S = N(L_O,T_S,e_O,t_C)$ in the loading-source temperature interval---is Young's modulus, agreeing numerically with Nielsen (34) and the

dynamic Young's moduli by Sorokin and Perepechko (33) and Crissman (35). Therefore, we confirm $e_O(L_O)$ at N_O as elastic strain (recall the texts of Figs. 3 and 4)

Thus, in Fig. 4, we see that N_O is a special point. At N_O, only the elastic strain responds to a DLL to $e_O(L_O)$ in t_C independent of temperature. Therefore, at $N_O = N(L_O,e_O)$, $e_O(L_O) = C$ for all T in the range $0\ K < T < T(Neck)$. This DLL to L_O in t_C only occurs with HS(MAX) = $(7.26\ cm)(e_O)/t_C = 120$ m/min. The model also suggests that $N_O = e_O(L_O)$ in the range $0 < T < T(Neck)$ for $t_L \leq t_C$ where $HS \geq HS(MAX)$.)

For the production of a whole TMT curve, DLL must occur in the loading-source temperature and time intervals (in the T_S-τ_S range wherein $N_S = N(L_O,T_S,e_O,HS[t_{LO}])$ and $e = e_O(L_O)$. Care must be used to differentiate the times involved. In this range there is no viscoelastic strain in either the TMT or CT associated with the applied L_O. Therefore, when an HDPE specimen undergoes a DLL to N_S at any $T_S \leq T_{SL} = 83$ K with any convenient $HS \leq HS(MAX)$ in the T_S-τ_S range, both the CT and TMT curves are represented by the elastic strain $e = e_O(L_O) = C$ which is independent of temperature, depending only on L_O. The resulting elastic-strain-only TMT curve is produced by a DLL in time t_{LO} with a proper $HS \leq HS(MAX)$ matched to a $\dot{T}_S$, where $T_S = \tau_S \dot{T}_S$.

In Figs. 3b and 5, while $T_{SL} = 83$ K fixes the upper limit of the TMT curve loading-source temperature interval $0\ K < T_S \leq T_{SL}$, the upper limit τ_{SL} of the TMT curve loading-source time interval $t_C \leq \tau_S \leq \tau_{SL}$ depends upon the applied $\dot{T}$ ($\tau_{SL} = T_{SL} / \dot{T} = 83 / \dot{T}$).

Although in the T_S-τ_S region, the position of N_S is dependent on HS as well as T_S and τ_S, the elastic strain $e_O(L_O)$ is the same at all N_S. At any given N_S, an elastic-strain-only TMT curve, having a definite $\dot{T}_S = T_S / \tau_S$, is manifested as an incipient whole TMT curve at T_{SL},τ_{SL}. That is, an elastic-strain-only TMT curve may be initiated at any loading-source point N_S in the T_S-τ_S region with a definite $\dot{T}_S$ matched to the DLL HS. It becomes a whole TMT curve in the T_O-τ_O region where $\tau_{SL} \leq \tau_O < \tau(Neck)$ and $T_{SL} \leq T_O < T(Neck)$. Therefore, a whole TMT curve may be initiated in the elastic-strain, T_S-τ_S region with $\dot{T}_S = \dot{T}_{S1}$ matched to HS, at any $N_S = N_{S1}$: for example, at $N_{S1} = N(L_O,T_{S1},e_O,HS[\tau_{S1}])$. Then, an elastic-strain curve-path passes through its initial point to the initial point of a whole TMT curve starting at $N_{SL1} = N(L_O,T_{SL1},e_O,\tau_{SL1})$ where $T_{SL1} / \tau_{SL1} = \dot{T}_{SL1}$. T_{S1} is set experimentally and τ_{S1} is determined with Eq. 2a. Then, from the experimental starting point N_{S1} in the T_S-τ_S region, an elastic-strain-only TMT curve path with $\dot{T}_{S1}$ matched to the DLL HS at N_{S1} will pass through N_{SL1}, where $\dot{T}_{S1} = \dot{T}_{SL1}$. At N_{SL1}, the elastic-strain-only TMT curve path started at N_{S1} becomes the path of the whole TMT curve; and, at N_{SL1}, it is implied that the correct $HS[\tau_{SL1}] = HS[\tau_{S1}]$ is retained for $\dot{T}_{SL1} = \dot{T}_{S1}$ to form the proper HS-$\dot{T}$ match.

Using the equation (not shown) of the line in Fig. 8, we obtain the maximum heating temperature rate $\dot{T}(MAX)$ = 3160 K/min to match HS(MAX) = 120 m/min. These values are the upper limits of the correct HS and $\dot{T}$ needed for a proper HS-$\dot{T}$ match for the limiting TMT curve that occurs at t_c and which is also an elastic-strain-only TMT curve in the model depicted by Figs. 3 and 5.

Therefore, in Figs. 3a, 3b, and 5 for all T in 0 K < T < T(Melt), the limiting TMT curve produced with $\dot{T}(MAX)$ = 3160 K/min has only the elastic strain $e_o(L_o)$ at the point N_o = $N(L_o,e_o,t_c)$ when a DLL is performed with HS(MAX) in $\tau = t_c$. In Fig. 3a, in the e-T plane, the limiting elastic-strain-only TMT curve produced with $\dot{T}(MAX)$ is $e_o(L_o)$. Likewise, in Fig. 3b, $e_o(L_o)$ is the limiting elastic-strain-only TMT curve in the e-τ plane. Similarly, a point at any T_o in the interval $T_{sL} \leq T_o < T(Melt)$ and $t_L = t_c$ is the starting point $N_o = N(L_o,T_o,e_o)$ of a CT N-path curve. The only access to a CT N-path at any N_o is through a DLL with HS = HS(MAX) in t_c (see Figs. 4 and 5).

Like the TMT curve, any CT curve below T_{sL}, initiated with any HS ≤ HS(MAX), results in a CT curve with only elastic strain $e_o(L_o) = C$.

Above T_{sL}, in the temperature range $T_{sL} < T_o < T(Melt)$, viscoelastic strain accompanies $e_o(L_o)$ in the CT curves as in theTMT curves.

The viscoelastic strain in a CT curve under dead-load above T_{sL} increases with time t at constant temperature, while, in a TMT curve under dead-load, it increases with T_o and τ_o at constant $\dot{T}$. Then, in the interval $T_{sL} < T_o < T(Neck)$, we describe each point on a TMT curve by an individual N(or P) = $N(L_o,T_o,e,\tau_o)$ where e is the Δ-adjusted total strain. We note from Figs. 3 and 4 that this N(or P) requires a proper HS-$\dot{T}$ match when a $\dot{T}$ is applied at T_o during an SM. What has been said for N(or P) holds at any point on the M surface in Fig. 5. The M surface is a constant load (or stress) surface on which there is CT and TMT DLL strain equivalence where, for 0 K < $T_s \leq T_{sL}$, $M_s = M(L_o,T_s,e_o,\tau_s)$ and $e = e_o(L_o) = C$, and for $T_{sL} < T_o <$ T(Neck), $M = M(L_o,T_o,e) = e = e_o(L_o) + e_{VE}(L_o,T_o,t_L\text{-}t_{Lo},\tau_o)$. Then, for 0 K < $T_{sL} < T_o <$ T(Neck), the SM is necessary and a proper HS-$\dot{T}$ match is required for undistorted whole TMT curves.

So far, we have seen that $e = e_o(L_o)$ at N_s in th T_s-τ_s region due to a DLL with HS < HS(MAX) in $t_L > t_c$; also at N_o, $e = e_o(L_o) = C$ for a DLL with HS = HS(MAX) in $t_{Lo} = t_c$ for all T, 0 K < T < T(Break).

The general literature, like that of Eisenstadt (36), indicates that the elastic strain, which is distortion of the carbon bonds in the backbone chain, is strain rate independent. We postulated this independence from Fig. 4 for the temperatures and loading rates considered and applied it in the above paragraphs. We also postulated that $e_o(L_o) = C$ independent of DLL to L_o with any HS ≥ HS(MAX) in $t_{Lo} \leq t_c$ and for any T in the range 0 K < T < T(Break).

From Fig. 4 (see also Figs. 3b and 5), the total strain at any N on the CT N-path---due to a DLL with an HS < HS(MAX) in $t_L > t_c$ for $T_o > T_{sL}$---in terms of its components is $e_o(L_o)$ + $e_{VE}(L_o,T_o,t_L$ $_{VE}(L_o,T_o,t_L-t_{Lo})$ which is the sum of the elastic and viscoelastic strains. e_{VE}, unlike e_o, is dependent upon T and HS. e_{VE} commences immediately after e_o is reached, provided HS < HS(MAX) and $t_L > t_c$ and $T_{sL} < T_o <$ T(Neck). e_{VE} is zero for any HS ≤ HS(MAX) and $t_L > t_c$ in the T_s range 0 K < T_s ≤ T_{sL}; and for HS = HS(MAX) in $t_{Lo} = t_c$ in the T range 0 K < T < T(Melt).

According to Billmeyer (37), the total strain, composed of elastic and viscoelastic components in a semicrystalline polymer, fully recovers if it is below the yield point. We found that his model holds for semicrystalline HDPE except we designate that full recovery apparently should occur only within the TT uniform strain limit that is well below the yield point (refer to the texts of Figs. 6 and 7).

We conclude that the CT-TMT DLL model, as presented in Figs. 3 and 5 and based upon the experimental results of Fig. 4 and pertinent references, gives reasonable and consistent explanations for all aspects of the DLL problem and related parameters.

Note that (according to Reference 33) not all polymers have a T_s-τ_s interval where, at N_s, e = e_o, so that, theoretically, the SM for a TMT with such polymers has T_{sL} at 4 K for the start of a whole TMT curve.

To experimentally show general TMT-CT LS equivalence at any N requires ranges of heating temperature rates and DLL strain rates for obtaining a full set of HS-$\dot{T}$ matches. Lacking this capability to establish TMT-CT LS equivalence over broad ranges, a search for other means, using the existing data and the experimental capability, exposed several useful phenomena. We will now illustrate these.

Only a fraction of the DLL initial strain rate was available to the specimen in its 2.54 cm gage length. This fraction results from the specimen effective-length between grips--6.36 cm in our case--(25)(38) and load-train softness. This fraction caused the loading curve, produced with the single HS offered by the creep apparatus of 0.127 m/min, to plot (see Fig. 4) with a lower HS near 1.27×10^{-2} m/min (0.5 in/min).

The other phenomenon is that of strain-rate skewing with temperature. Above 20°C specimens soften. This softening with higher temperature decreased the specimen effective-length between grips. Relative to the given HS, softening caused a skewing of the DLL curves to shorter loading times and to higher DLL initial strain-rate. Temperatures below 20°C stiffen the specimen. This stiffening at lower temperatures increased the specimen effective-length causing the loading curve to skew to the right--to lower initial, DLL strain-rates relative to the given HS. We see such skewing in the DLL curves in Fig. 4. The TMT curves, to match these skewed initial, DLL strain-rates, require constant heating temperature rates greater than 4 K/min that

were not available with the present apparatus. Therefore, we needed a procedure to replace the more direct, but unavailable, experimental devices for obtaining proper HS-$\dot{T}$ matches.

The procedure we used was to make a TMT e-T curve with a varying $\dot{T}$. This TMT curve consisted of a monotonically-decreasing $\dot{T}$ along its path, with the initial heating temperature rate greater than 4 K/min. To make such a TMT curve required cooling the specimen with cold nitrogen gas. In conjunction with cooling from 20°C to -60°C, we produced a puddle of liquid nitrogen on the floor of the EC. At -60°C, the specimen reached thermal equilibrium. Then, using the SM, we loaded the specimen at -55°C with the existing HS of 0.127 m/min. This resulted in an effective HS of 0.0127 m/min. We stopped the supply of liquid nitrogen to the puddle and heated the specimen from this low temperature to the desired end temperature. The cold nitrogen gas and the liquid nitrogen puddle depleted as the interior of the EC warmed due to a constant supply of heat from a 1200 watt source. In this manner, we produced a TMT curve with a monotonically decreasing $\dot{T}$ between -55°C and 70°C. At -55°C, this $\dot{T}$ was 8 K/min. It decreased to 3.5 K/min at the 70°C end where we terminated the TMT. We produced two TMT e-t curves with this nonconstant-$\dot{T}$ technique: one with a load of w(i) which has an unknown HS, and, the other with L_o = w(i) + W(EX) with a stress of 9.19 MPa. We do not show these "manually produced" TMT curves. Analysis of these curves produced N-points that we superimposed on the isotherms of Figs. 1 and 4 at the corresponding strains and temperatures (solid squares) from which we produced Fig. 8. Fig. 8 shows matched HS-$\dot{T}$ pairing. As Fig. 8 represents proper HS-$\dot{T}$ pairs, not N-points, each solid square is identifiable only if the $N(L_o,T_o,e)$ corresponding to it from Fig. 4 is explicitly tagged in Fig. 8. Furthermore, Fig. 8 is a sampling produced with only a single HS-$\dot{T}$ point (solid square) from each N-path isotherm in Fig. 4. Therefore, the Fig. 8 HS-$\dot{T}$ data, collected from a TMT with a nonconstant heating temperature rate, attests to the existence of more general matching results. We would expect such general matching results from a set of TMT curves, performed at one stress level, with each curve of the set with its own constant heating temperature rate. Obtaining such TMT sets of curves requires apparatus capable of dealing with HS and $\dot{T}$ ranges over a large span of Fig. 5.

In a TMA test, the measurement of the thermal strain due to α requires an external load however minute. The total strain consists of the thermal strain due to αT_o plus that due to the minute load. We depict tthe total strain by Eq. 1, if w(i) is the minute load. Care should be taken so as not to attribute the total strain alone to the first term ignoring the existence of the other terms of Eq. 1. Thus, just as in the TMT, there may exist in the TMA the problem of separating the thermal component of strain from the mechanical component. Though the mechanical strain component is very small, it may make a significant contribution in the temperature range above room temperature (RT); $RT \le T_o < T(Neck)$.

From the experiments depicted in Figs. 1 and 2, we saw that the thermal strain, due to α alone, was not obtainable directly because it was accompanied by the strain due to w(i). This is a consequence of present apparatus limitations. It is seen from the following paragraph that for a

TMT with w(i) = 13.2 Newton, which would be a prohibitively large load for a conventional TMA apparatus, there still is a graphically observable connection with dynamic testing as well as with the TMA.

Δ, the total strain of the TMT curve in Fig. 1, expressed by Eq. 1, consists of thermal and mechanical strain. Even with a much larger mechanical strain component than a TMA, Δ has a visible inflection point near 41°C (at the large black dot). An inflection point also appeared at 41°C in our TMA scan (not shown) of the thermal strain versus temperature for HDPE. In addition, we noted an inflection point at 41°C on the dynamic loss modulus (not shown) for this material. There also was an inflection point for polyethylene oriented parallel to the loading direction at 40°C, by Takayanagi et al. (39), which is reproduced in Nielsen (34). Also, the inflection point in the dynamic data of Hu, et al. (40) for oriented HDPE occurred at 40°C.

In attempting to answer questions like those stated at the start of the DISCUSSION section, we examined TT loading in the role of a loading method for initiating the TMT or the CT. The TT loading method, however, has restrictions as a loading mode for CT/ TMT loading. The TT load-strain curve is strictly a loading curve to its end. The TT loading has a discontinuity in strain rate at R (and Q) between the constant crosshead speed loading path and the quasi-creep R-path when used as a loading mode for a CT or a TMT.

Alden (41) also observed a discontinuity in strain rate when loading metals for creep with his specialized apparatus, so that his loading mode appears to be like the TT loading mode in this respect.

Although the anomalous TT-CT-TMT LS equivalence exists, the TT loading is not a substitute for a DLL to N. Away from Q, the response of the specimen to a TT loading is along the R-path, not the N-path. We conclude that the TT loading mode is a special mode for a CT or TMT, producing a strain-time R-path different from that produced by a DLL to the N-path except at the point Q.

While the TT is not a general loading mode for a TT-CT-TMT LS equivalence, some interesting thermodynamic features are suggested by the differing N- and R-paths. Except at Q, Fig. 4 shows that LS inequality exists between N and R elsewhere. We perceive this inequality to be due to differing thermodynamic paths of loading with a consequent difference in moduli (the adiabatic DLL path leads to N on the CT N-path; the isothermal TT loading path leads to R on the R-path). We see the resulting adiabatic and isothermal moduli to be temperature and loading rate dependent along their respective paths. Schrieber et al. (42) presents the thermodynamics for the adiabatic and isothermal moduli and their difference. Their difference is called the modulus defect (ΔE) by Cottrell (43). For any temperature, ΔE is largest at t_c, between $N_o = N(L_o,T_o,e_o,t_c)$ and $R_o = R(L_o,T_o,e,t_c)$, decreasing to zero at Q.

The isothermal moduli on the TT R-paths in Fig. 4 are secant moduli as the TT uniform strain involves strain consisting of both elastic and viscoelastic strains. These isothermal secant moduli, calculated from stress and strain at R along the constant temperature R-path, are found equal to ASTM moduli. For example, at 20°C, with a crosshead speed of 0.127 m/min, and a

stress of 9.19 MPa, E[isothermal R-path]] = E[ASTM within 6%. The E[ASTM] is from the HDPE data of Hartmann et al. (44) with the corresponding strain plotted in Fig. 4.

The elastic e_0 at t_c--at the start of the extrapolated adiabatic N-path---results in a calculated modulus $E_0(T_s) = 1.03 \times 10^4$ MPa, in agreement with the dynamic Young's modulus or "instantaneous" Young's modulus in the literature for HDPE.

If the activation enthalpy ΔH for HDPE is set to zero in the Bucci-McCrum (26) compensation equation, then $t = t_c$ and $e = e_0$ for all T, including 0 K. t_c is consistent (according to Fig. 4) with results from isothermal creep-strain N-paths extrapolated to a common point $N_0 = N(L_0,e_0,t_c) = C$ for all temperatures. The Bucci-McCrum compensation time effects recounted here for HDPE were presented by Warnas (45).

The use of streamlined tensile specimens (SL) did not compromise the generality of the tests but, whatever type the specimen, the initial total length between grips was important. Whatever this length is, since it affects the strain rate in the specimen, it should be the same for each test in the regimen and one should report it along with the gage length.

We expect the experimental techniques in this paper to hold for amorphous materials such as polycarbonate and to that extent we consider them to be general for thermoplastics.

FUTURE WORK

Since we do not know any proper HS-$\dot{T}$ matches without experiment, we require ranges of loading rates and heating temperature rates to fill in the experimental gaps needed to prove the theoretical limits in Figs. 3, 5 and 8. This requires replacement or modification--like that mentioned by Baxter (46)--of the present experimental apparatus to accommodate a range of loading rates and a range of linear temperature rates, perhaps to 100 K/min.

As the loading of a specimen with only w(i) precludes the use of the SM and has other undesirable affects on the specimen, it is desirable to eliminate this ever-present, intrinsic load produced by the extensometer, perhaps by replacement with an optical system (46).

Of future interest is the investigation of the relationships of the isothermal R-path and the adiabatic N-path from the point of view of thermodynamics and continuum mechanics, perhaps along the lines suggested by the work of Paglietti (47).

Also of interest is the Hopkinson pressure bar experiment of Davies and Hunter (48) as performed on low density polyethylene in the t_{Lo} interval $t_{Lo} < t_c$, where an elastic strain is indicated in a reasonable proportion to that for HDPE. It would be of interest to do this experiment with HDPE to see whether $N_o = e_o(L_o) = C$ for t_{Lo} in any part of the interval $0 < t_{Lo} < t_c$, independent of temperature.

ACKNOWLEDGMENTS

Thanks go to Mr. Marc S. Pepi and to Mr. Robert E. Pasternak, of MTL, Materials Testing and Evaluation Branch; the former, for sharing with me in the production of the TMT and TT curves, and the latter for discussions on several types of tension machines.

Thanks go to Dr. Bernard M. Halpin, Chief, and to Dr. Richard J. Shuford, Group Leader, of MTL, Composites Development Branch, for support of the Loading Project and, in the writing of this paper during my tenure as emeritus at MTL.

NOMENCLATURE

α	Coefficient of linear thermal expansion
Δ	Total strain in a TMT (or CT) curve with w(i) and α
ΔE	Modulus decrement
η_{ex}	Troutonian, or extensional, viscosity
τ	TMT N-path time in e-τ plane reckoned from t_c
τ_s	TMT curve time in $t_c \leq \tau_s \leq \tau_{sL}$
3-D	Three-dimensional
^oC	Centigrade temperature
CT	Creep test
DLL	Dead-load loading
E_o	Young's modulus
e	Total engineering strain (loading strain)
$e_o(L_o)$	Elastic strain due to a full dead-load L_o
e_{VE}	Viscoelastic strain in a TMT or CT curve
de / dt	N-path creep strain rate
de / dt_L	CT/TMT DLL strain rate to N; also TT loading strain rate to R
de / dτ	Time rate of strain on a TMT curve in the e-τ plane (= $\dot{e}$)
de / dT	Thermal rate of strain on a TMT curve in the e-T plane (= e')
EC	Environmental chamber
HDPE	High density polyethylene
HS	Initial speed (initial crosshead speed)
HS(MAX)	Maximum Initial speed (=120 m/min)
K	Absolute temperature degree
L	Load in TT L-e plane
L_o	Dead load
LS	Loading strain
M	CT-TMT LS point in 3-D
M_o	CT-TMT LS point in 3-D due to HS(MAX) in t_c
M_s	TMT LS point in 3-D in the T_s-τ_s region
M_{sL}	TMT LS point in 3-D in the T_{sL}-τ_{sL} region
N	CT-TMT LS point in the e-t_L or e-τ plane
N_o	M_o component in the e-t_L or e-τ plane at t_c
N_s	M_s component in the e-τ plane
N_{sL}	M_{sL} component in the e-τ plane
P	TMT LS point in the e-T plane
P_o	M_o component in the e-T plane
P_s	M_s component in the e-T plane
P_{sL}	M_{sL} component in the e-T plane
PMMA	Poly(methylmethacrylate)
Q	LS point for CT-TMT-TT equivalence
R	TT point in e-t_L (and L-e) plane

SL	Streamlined tensile specimen
SM	Synchronization maneuver
t	N-path creep-strain time
t_C	Compensation time (34×10^{-6} s)
t_{oL}	Initial loading time (= 0)
t_{Lo}	DLL time to $e_o(L_o)$
t_L	CT, TMT, and TT loading times (to N and R) in the e-t_L plane
T	General temperature
T_o	Temperature in the range $T_{sL} < T_o < T(Melt)$
T_s	Temperature in the range $0\ K < T_s \leq T_{sL}$
T_{sL}	Temperature at the start of a whole TMT curve (= 83 K)
T(Melt)	Melting temperature of HDPE (413 K)
TDA	Thermodilametric analysis
TMA	Thermomechanical analysis
TMT	Thermomechanical test
TMT(TT)	Thermomechanical test from TT data
$\dot{T}$	Heating-cooling temperature rate = $dT / d\tau$
$\dot{T}(MAX)$	Maximum $\dot{T} = (dT / d\tau)(MAX) = 3{\cdot}160$ K/min
TT	Engineering tensile test; Instron tensile test
w(i)	Extensometer weight contribution to L_o
W(EX)	Iron-weight contributions to L_o

REFERENCES

1. \ T DiBenedetto, and K.L. Trachte, J. App. Polymer Sci., Vol. 14, 2249, (1970).
2. I.V. Yannas, J. Macromolecular Science-Physics B6, Vol. 91, 1623, (1972).
3. G.L. Dieter, Mech. Metallurgy, 2nd ed., Section 8.2 McGraw-Hill, New York, NY (1976).
4. S. Turner, Polymer Eng. and Sci., 306-316, October (1966).
5. R.A. Shapery, Polymer Eng. and Sci., 295-310, July (1969).
6. C. Bauwens-Crowett, and J.C. Bauwens, J. of Mat. Sci., Vol. 10, 1778, (1975).
7. S.B. Ratner, and E.K. Krasnova, Mech. of Comp. Materials (Eng. Trans.), No. 5, 550, Sept., (1986).
8. L.E. Nielsen, Mechanical Properties of Polymers and Composites, Vol. 2, Ch. 5, Dekker, New York, NY. (1974).
9. M.T. Watson, G.M. Armstrong, and W.D. Kennedy, Modern Plastics, 161, Nov., (1956).
10. J.W. Liska, Ind. Eng. Chem., Vol. 36, 40, (1944).
11. B. Bossu, M. Chatain, P. DuBois, and J. Rougeaux, ASTM Spec. Tech. Pub., No. 247.
12. V.A. Kargin, and T.L. Sugolova, Zhfkh., Vol. 23, 530, (1949).
13. G.L. Slonimskii, A.A. Askadskii, and V.I. Pavlov, Polymer Mech. (Eng. Trans.), Vol. 2, 460, (1966).
14. G.L. Slonimskii, and A.A. Askadskii, Polymer Mech. (Eng. Trans.), Vol. 1, 40, (1975).
15. V.N. Efimova, and R.D. Maksimov, Polymer Mech. (Eng. Trans.), No. 2, 196, (1977).
16. A.A. Askadskii, TV. Toddled, and E.G. Gal'pern, Mech. of Comp. Materials (Eng. Trans.), No. 6, 665, (1984).
17. V.N. Borsenko, A.B. Sinani, and V A. Stepanov, Polymer Mech. (Eng. Trans.), Vol. 4, 19, (1968).
18. E.V. Minkin, M.P. Lewnovskii, S.T. Semenets, and Y.V. Zelenov, Polymer Mech. (Eng. Trans.), No. 4, 619, (1972).
19. O.S. Brüller, and H.H. Schmidt, Polymer Eng. and Sci., Vol. 19, No. 12, (1979).
20. R.A. Shapery, and Y.C. Lou, Glass Reinforced Epoxy Systems, Materials Tech. Series, J.C. Hilado, ed., Vol. 2, 92, Technical Publishing Co., Westport, CT.
21. A.T. Riga, Polymer Eng. and Sci., Vol. 14, No. 11, Nov., (1974).
22. R.E. Robertson, App. Polymer Symp., Vol. 7, 201, (1968).
23. G.M. Bryant, Textile Research J., Vol. 31, 399, (1961).
24. R.D. Andrews, and Y. Kazima, J. App. Phys., Vol. 38, 4118, (1967).
25. A.A. Warnas, and M.S. Pepi, U.S.Army Materials Technology Lab., TR 90-34, Watertown, MA 02172-0001.
26. N.G. McCrum, Polymer, Vol. 25, 299, (1984).
27. D.W.Oplinger, B.S.Parker, C.R. Gandhi, R.LaMothe, and G.Foley, ASTM STD, No. 864, (1985).
28. A.Schwartz, J. Therm. Anal., Vol. 13, 489, (1978).
29. S.Strella, High Speed Testing, Vol. 1, Intersci. Pub., Inc., New York, NY, 27, (1960).
30. J.B.Conway, Numerical Methods for Creep Rupture Analysis, Introduction, Gordon and Breach, eds., New York, NY. (1973).
31. R.D.Maksimov, E.A.Sokolov, and V.P. Mochalov, Polymer Mech. (Eng. Trans.), No. 32, 334, May-June, (1975).

32. V.N.Borsenko, N.N.Peschanskaya, A.B.Sinani, and A.P.Stepanov, Polymer Mech. (Eng. Trans.), No. 1, 19, Jan.-Feb., (1970).
33. V.E.Sorokin, and I.I.Perepechko, Polymer Mech. (Eng. Trans.), Vol. 10, 14, (1974).
34. L.E.Nielsen, Mechanical Properties of Polymers and Composites, Vol. 1, Table 3, 207, Dekker, NY, (1974).
35. I.M.Crissman, I.A.Sauer, and A.E.Woodward, J. Polymer Sci., Vol. A2, 5075, (1964).
36. M.M.Eisenstadt, Introduction to Mehanical Properties of Materials, p. 264 (Figs. 8 through 44), and p. 306 (Question 4), MacMillan, NY, (1971).
37. F.W. Billmeyer, Jr., Textbook of Polymer Science, 2nd ed., Chapt. 6, Wiley & Sons, New York, NY, (1971).
38. A.F.Yee, and P.D.Detorres, Polymer Eng. and ScI., 691, Oct., (1974).
39. Takayanagi, Imada, and Kajiyama, J. Polymer Sci., Vol. C15, 263, (1966).
40. S-R Hu, T.Kyu, and R.S.Stein, J. Polymer Sci., Part B, Polymer Physics, Vol. 25, 71, (1987).
41. T.A. Alden, Mat. Sci. and Eng., Vol. A103, 213, (1988).
42. E.Schrieber, O.L.Anderson, and N.Soga, Elastic Constants and Their Measurement, Sect. 2.6, McGraw-Hill, New York, NY, (1973).
43. A.H.Cottrell, Mechanical Properties of Matter, 178, Wiley & Sons, New York, NY, (1964).
44. B.Hartmann, G.F.Lee, and R>F.Cole, Polymer Eng. and Sci., 554, April, (1986).
45. A.A.Warnas, Polymer Communications, Vol. 32, No.3, 83, (1991).
46. F.D.Baxter, Advanced Mats. and Processes, Vol. 139, No. 2, 21, Feb., (1991).
47. A.Paglietti, Int. J. of Non-Linear Mechs., Vol. 24, 571, (1989).
48. E.D.H.Davies, and S.C.Hunter, J. Mech. Phys. Solids, Vol. 11, 155, (1963).

DISTRIBUTION LIST

No. of Copies	To
1	Office of the Under Secretary of Defense for Research and Engineering, The Pentagon, Washington, DC 20301
	Director, U.S. Army Research Laboratory, 2800 Powder Mill Road, Adelphi, MD 20783-1197
1	ATTN: AMSRL-OP-SD-TP, Technical Publishing Branch
1	AMSRL-OP-SD-TA, Records Management
1	AMSRL-OP-SD-TL, Technical Library
	Commander, Defense Technical Information Center, Cameron Station, Building 5, 5010 Duke Street, Alexandria, VA 23304-6145
2	ATTN: DTIC-FDAC
1	MIA/CINDAS, Purdue University, 2595 Yeager Road, West Lafayette, IN 47905
	Commander, Army Research Office, P.O. Box 12211, Research Triangle Park, NC 27709-2211
1	ATTN: Information Processing Office
	Commander, U.S. Army Materiel Command, 5001 Eisenhower Avenue, Alexandria, VA 22333
1	ATTN: AMCSCI
	Commander, U.S. Army Materiel Systems Analysis Activity, Aberdeen Proving Ground, MD 21005
1	ATTN: AMXSY-MP, H. Cohen
	Commander, U.S. Army Missile Command, Redstone Arsenal, AL 35809
1	ATTN: AMSMI-RD-CS-R/Doc
	Commander, U.S. Army Armament, Munitions and Chemical Command, Dover, NJ 07801
1	ATTN: Technical Library
	Commander, U.S. Army Natick Research, Development and Engineering Center Natick, MA 01760-5010
1	ATTN: SATNC-MI, Technical Library
	Commasnder, U.S. Army Satellite Communications Agency, Fort Monmouth, NJ 07703
1	ATTN: Technical Document Center
	Commander, U.S. Army Tank-Automotive Command, Warren, MI 48397-5000
1	ATTN: AMSTA-ZSK
1	AMSTA-TSL, Technical Library
	President, Airborne, Electronics and Special Warfare Board, Fort Bragg, NC 28307
1	ATTN: Library
	Director, U.S. Army Research Laboratory, Weapons Technology, Aberdeen Proving Ground, MD 21005-5066
1	ATTN: AMSRL-WT

No. of Copies	To
	Commander, Dugway Proving Ground, UT 84022
1	ATTN: Technical Library, Technical Information Division
	Commander, U.S. Army Research Laboratory, 2800 Powder Mill Road, Adelphi, MD 20783
1	ATTN: AMSRL-SS
	Director, Benet Weapons Laboratory, LCWSL, USA AMCCOM, Watervliet, NY 12189
1	ATTN: AMSMC-LCB-TL
1	AMSMC-LCB-R
1	AMSMC-LCB-RM
1	AMSMC-LCB-RP
	Commander, U.S. Army Foreign Science and Technology Center, 220 7th Street, N.E., Charlottesville, VA 22901-5396
3	ATTN: AIFRTC, Applied Technologies Branch, Gerald Schlesinger
	Commander, U.S. Army Aeromedical Research Unit, P.O. Box 577, Fort Rucker, AL 36360
1	ATTN: Technical Library
	U.S. Army Aviation Training Library, Fort Rucker, AL 36360
1	ATTN: Building 5906-5907
	Commander, U.S. Army Agency for Aviation Safety, Fort Rucker, AL 3636
1	ATTN: Technical Library
	Commander, Clarke Engineer School Library, 3202 Nebraska Ave., N., Fort Leonard Wood, MO 65473-5000
1	ATTN: Library
	Commander, U.S. Army Engineer Waterways Experiment Station, P.O. Box 631, Vicksburg, MS 39180
1	ATTN: Research Center Library
	Commandant, U.S. Army Quartermaster School, Fort Lee, VA 23801
1	ATTN: Quartermaster School Library
	Naval Research Laboratory, Washington, DC 20375
1	ATTN: Code 6384
	Chief of Naval Research, Arlington, VA 22217
1	ATTN: Code 471
	Commander, U.S. Air Force Wright Research and Development Center, Wright-Patterson Air Force Base, OH 45433-6523
1	ATTN: WRDC/MLLP, M. Forney, Jr.
1	WRDC/MLBC, Mr. Stanley Schulman
	U.S. Department of Commerce, National Institute of Standards and Technology, Gaithersburg, MD 20899
1	ATTN: Stephen M Hsu, Chief, Ceramics Division, Institute for Materials Science and Engineering

No. of Copies	To
1	Committee on Marine Structures, Marine Board, National Research Council, 2101 Constitution Avenue, N.W., Washington, DC 20418
1	Materials Sciences Corporation, Suite 250, 500 Office Center Drive, Fort Washington, PA 19034
1	Charles Stark Draper Laboratory, 555 Technology Square, Cambridge, MA 02139
	Wyman-Gordon Company, Worcester, MA 01601
1	ATTN: Technical Library
	General Dynamics, Convair Aerospace Division, P.O. Box 748, Fort Worth, TX 76101
1	ATTN: Mfg. Engineering Technical Library
	Plastics Technical Evaluation Center, PLASTEC, ARDEC, Bldg. 355N, Picatinny Arsenal, NJ 07806-5000
1	ATTN: Harry Pebly
1	Department of the Army, Aerostructures Directorate, MS-266, U.S. Army Aviation R&T Activity - AVSCOM, Langley Research Center, Hampton, VA 23665-5225
1	NASA - Langley Research Center, Hampton, VA 23665-5255
	U.S. Army Vehicle Propulsion Directorate, NASA Lewis Research Center, 2100 Brookpark Road, Cleveland, OH 44135-3191
1	ATTN: AMSRL-VP
	Director, Defense Intelligence Agency, Washington, DC 20340-6053
1	ATTN: ODT-5A, Mr. Frank Jaeger
	U.S. Army Communications and Electronics Command, Fort Monmouth, NJ 07703
1	ATTN: Technical Library
	U.S. Army Research Laboratory, Electronic Power Sources Directorate, Fort Monmouth, NJ 07703
1	ATTN: Technical Library
	Director, U.S. Army Research Laboratory, Watertown, MA 02172-0001
2	ATTN: AMSRL-OP-WT-IS, Technical Library
5	Author